RESEARCH ARTICLE OPEN ACCESS

A review on corrosion protection of metals and alloys by thermal spraying coatings

Victor C. Campideli[1], Hana H. Koga[1], Dalila C. Sicupira[1], Vanessa F. C. Lins[2]
[1]*Department of Chemistry, Universidade Federal de Ouro Preto, Phone: + (55) (31)35591282, Campus Morro do Cruzeiro, Ouro Preto, MG 35400-000, Brazil*
[2]*Department of Chemical Engineering, Universidade Federal de Minas Gerais, Belo Horizonte, MG 31270-901, Brazil.*

Abstract
The thermal spraying technique has been developed for over a century. During this time, the technique has been enhanced, and it has gained a great deal of interest in society due to its many applications in the industrial field: textile, aerospace, chemical industries, automotive, and others. Recently, many applications related to corrosion protection with thermal spray coating have been improved using different techniques such as flame spraying (FS), atmospheric/vacuum plasma spraying (APS/VPS), arc spraying (ARC), detonation gun spraying (DGS), cold spraying (CS), high-velocity air fuel spraying (HVAF) and high-velocity oxy-fuel spraying (HVOF). In this paper, a review of corrosion protection by thermal spray coatings has been done along with its latest innovations.
Keywords: Thermal spraying; Corrosion; Coatings; Cold spraying; Arc Spraying; Atmospheric plasma spraying; Detonation gun spraying; HVOF

Date of Submission: 05-01-2025 Date of acceptance: 16-01-2025

I. Introduction

The thermal spray technique is an effective and low-cost solution to mitigate corrosion. Protecting the substrate with a coating avoids the necessity of frequent repair by extending the life of the material through the application of an effective coating that separates the substrate from the environment. A disadvantage of the thermal spraying technique is the porosity of the coatings, which impairs their resistance to corrosion and wear. However, the literature reports the use of sealants whose efficiency has been proven through corrosion evaluation tests [1]. Due to the high deposition rate, repair capacity, and wide range of materials available to use in the coating, the thermal spray technique is applied in the textile, energy, petroleum, aerospace, automotive industries, among others [2]. The thermally sprayed coating's lamellar structure is an important characteristic that reduces the entry of aggressive agents through the coating to the substrate forcing aggressive agents to have a longer and more tortuous path to the substrate.

In general, the thermal spray concept can be defined by multiple impacts of molten or semi-molten droplets at a certain velocity on a substrate, followed by lateral flattening, fast solidification, and cooling [3]. Throughout the years, several techniques were developed and can be classified according to the material properties such as combustion, cold spray, and electrical energy, which include arc and plasma [4].

Recently, much effort has been applied to developing thermal spraying techniques. The different techniques used in recent studies are flame spraying (FS), atmospheric/vacuum plasma spraying (APS/VPS), arc spraying (ARC), detonation gun spraying (DGS), cold spraying (CS), high-velocity oxy-fuel spraying (HVOF) and high-velocity air fuel spraying (HVAF). According to the particle velocity and deposition temperature, the thermal spray techniques can be represented as shown in Figure 1.

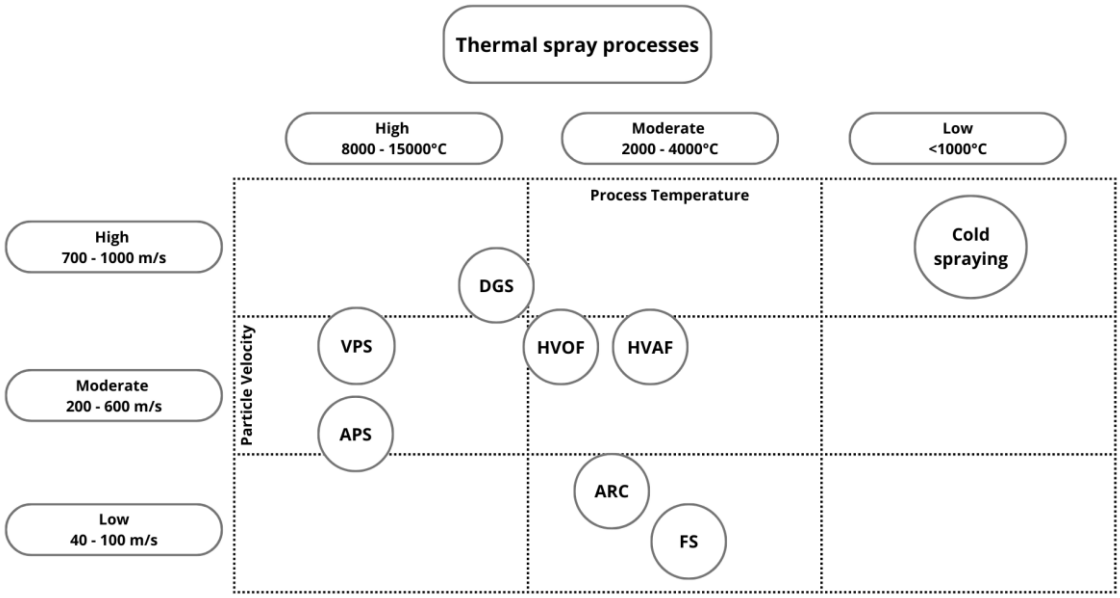

Figure 1: Types of thermal spray techniques: (FS) flame spraying, (APS/VPS) atmospheric/vacuum plasma spraying, (ARC) arc spraying, (DGS) detonation gun spraying, cold spraying, (HVOF) high-velocity oxy-fuel spraying and (HVAF) high-velocity air fuel spraying (Adapted from Berger, 2007)[5].

Thermal spraying technology has been developed and enhanced since the early 1900s when Dr. Schoop (1911) performed his first experiments using molten and powdered metals. In 1912, his effort produced the first device based on the principle of a wire rod put into contact with a concentrated flame, which had fuel gas with oxygen; it melted, and the flame, surrounded by a stream of compressed gas, would molt the metal and become atomized and readily propelled onto a surface to create a coating. This technique is known as flame spraying (FS) [6].

On the other hand, the atmospheric/vacuum plasma spray process (APS/VPS) has a general operation that includes introducing feedstock powders into a plasma stream [7]. Subsequently, the molten or semi-molten forms of powders would be projected onto a substrate, followed by flattening, rapid solidification, and cooling. So, these molten particles produce overlapping splats coating the substrate. The spraying can be conducted in air, low pressure, or vacuum [8].

In the case of the arc spray process (ARC), two metallic wires are fed at controlled speed into the arc gun and electrically charged with positive and negative polarity. Until the point where the two wires come into contact, an electric arc is created, which melts the wires. Compressed gas steam accelerates the molten particles toward the surface of the tube and forms the coating [9]. This technique has the feasibility of depositing thick coatings on large surfaces at a relatively low cost. Also, it offers high bond strength (2 to 3 times greater than flame spray), low heat input, a denser coating (compared to flame spray), high spray efficiency, a high deposition rate, and no expensive gas such as argon is required [10, 11].

Another process known as detonation gun spray (DGS) provides good adhesive strength, low porosity, and a coating surface with compressive residual stresses [12]. A quantity of oxygen and acetylene is measured and fed through a tubular barrel closed at one end. To prevent a backfire, nitrogen gas is allowed to cover the gas inlets. At the same time, a quantity of the coating powder is added to the combustion chamber. The gas mixture inside the chamber reacts, resulting in the combustion of the gas mixture and generating a high-pressure shock wave (detonation wave), which propagates through the gas stream [13].

In contrast, the cold spray process is based on low-temperature, high-velocity jets propelling material. Therefore, there is no heat source, only hot compressed gases that are fed into a gun with a lava nozzle, resulting in a coating with a low oxidation level, high density, and enhanced adhesion [6].

Also at high particle velocities, high-velocity oxy-fuel (HVOF) thermal spray is a process with low gas temperatures [14]. It presents four main physical-chemical processes occurring in the thermal and flow fields. In the combustion chamber, fuel oxidation turns chemical energy into thermal energy, which is converted into kinetic energy by expansion through the nozzle and energy transfer

from the particles during the expansion processes. The nozzle outlet and atmospheric pressure affect the free jet flow field, and the kinetic and thermal energy are converted into work and surface energy at coating deposition [15].

Besides, the high-velocity air-fuel (HVAF) spray process is used for the deposition of metallic and carbide-metal coatings on powder materials. The sprayed particles are heated below their melting point and accelerated to a velocity well above 700 m/s to form dense and non-oxidized deposits with minimal thermal deterioration and outstanding technology efficiency. Thus, this is a solid particle spraying technology in which particle temperature remains an important factor in coating formation [16].

Recently various researchers have proposed methods to improve the corrosion resistance of metals, and thermal spray technologies have become an important alternative to improve product life span [12, 13, 17-19]. In the following, the results obtained by some researchers have been discussed.

II. Current state of the art and trend of the thermal spraying techniques

2.1. Flame Spraying (FS)

The flame spraying technique has the capacity to form surfaces with adequate roughness, forming a coating with lamellar structure, at a lower cost than plasma or HVOF spray techniques [20-23]. However, compared with other methods such as HVOF and plasma spraying, flame spray operates with a lower temperature and a lower spray velocity, producing coatings with a higher porosity and a lower bond strength [24], which is detrimental to the corrosion resistance of the flame-coated substrate in several media. A schematic drawing of the flame spray technique containing the main variables is shown in Fig. 2.

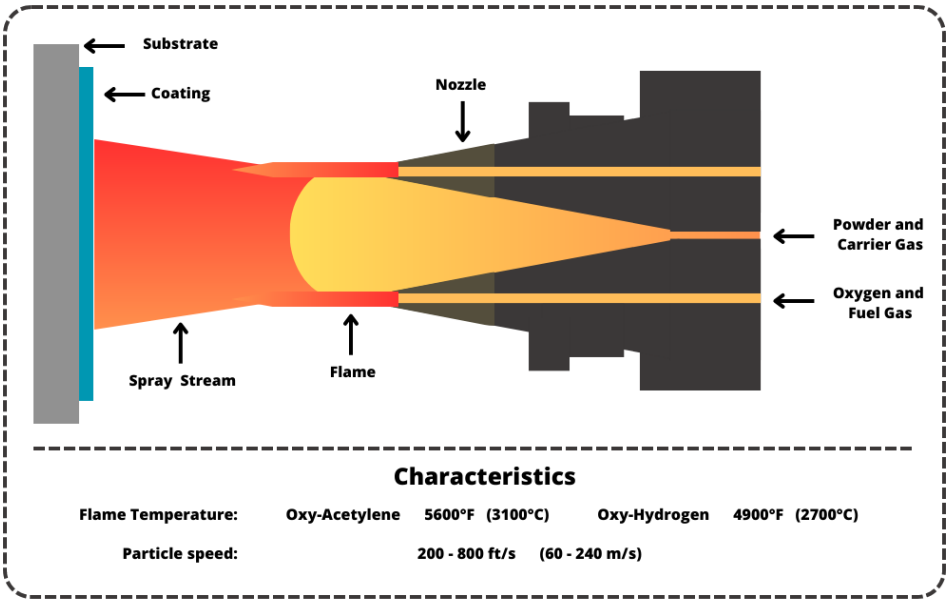

Figure 2. A scheme of the flame spraying technique

Nickel-chromium coatings [25] were plasma- and flame-sprayed onto a stainless-steel surface to protect it from high temperatures in power plant boilers. The porosity and oxide fraction of coatings depend on the deposition method used (plasma or flame spraying). The flame-sprayed NiCr coatings showed a higher porosity and oxide fraction than the plasma-sprayed coatings. A lower substrate adhesion was obtained in the flame sprayed coatings, even with a NiMoAl bond coat [25]. The greater porosity and lower adhesion to the substrate of flame-sprayed coatings negatively affects their resistance to corrosion in each environment.

Redjal et al. [26] studied the characterization of thermal flame sprayed coatings prepared from FeCr mechanically milled powder. The application of a milled powder allows for a

reduction of the porosity of the coating to 2-3%, while in flame-sprayed coatings, the porosity is usually between 10% and 20%. Thus, the use of milled powder in flame spray coatings is beneficial to the coating's corrosion resistance. This study showed that the mechanical and electrochemical properties of FeCr thermal spray coatings depend on the coating thickness, which ranged from 190 µm to 1500 µm, the substrate roughness, the Ni-based bond coating, and polymer sealing. The application of a Ni-based coating or sealing with a polymer improves the corrosion resistance of coatings [24]. The authors selected the thermal spraying technique to enable the deposit of thicker coatings, comparing it with techniques such as magnetron sputtering. However, they observed that chromium concentration was higher in thinner coatings (300 µm), which offered greater corrosion protection and reduced corrosion current densities than the substrate of mild steel. One interesting result is that the coatings of 700 µm and 1200 µm in thickness showed higher corrosion current densities than the uncoated steel. The open circuit potential values of coatings were lower than those of the mild steel substrate, but this parameter should not be considered in isolation.

Flame spraying has proven to have great potential for the formation of amorphous coatings with excellent anticorrosive properties [21, 22]. Si et al. [22] studied the corrosion resistance of an amorphous coating of Fe-Mo-Cr-Co sprayed with subsonic flame (SBFS), performing the deposition of an amorphous coating based on a low-cost Fe-based coating on a 316L stainless steel. This technique typically presents the main defects of pores and interlamellar cracks, which are structural defects that occur in the coating made by spraying with a subsonic flame. But there are no pores at the substrate/amorphous coating interface. It is necessary to optimize the technique to avoid the occurrence of undeformed particles that may cause these defects. The Fe-Mo-Cr-Co coatings showed a wider passive region and a higher breakdown potential than the stainless-steel substrate in a 3.5% NaCl aqueous solution [22]. The authors did not discuss the effect of Co on the corrosion resistance of the coating in a saline solution. Both AISI 316 steel and its coating contain elements like Fe, Cr, and Mo. The beneficial effect of Cr and Mo elements on the corrosion resistance of metallic alloys is well known. The amorphous state of the coating increases the coating's corrosion resistance compared to polycrystalline steel, since in the amorphous coating there are no high-energy anodic regions such as grain boundaries.

Kong et al. [21] also used SBFS to produce an amorphous FeCoCrMoSi coating, and they studied its corrosion resistance in NaCl solution at 3.5 wt.%. The use of supersonic flame spray (SPFS) was due to its lower temperature (below 3000 °C), which is beneficial for inhibiting the crystallization of amorphous powders. The spraying of FeCoCrMoSi was carried out by means of a vacuum gas that contained Co, Cr, Mo, and Si, using a spray gun 200 mm from the substrate. The coating had a high amorphous content. The open circuit potential decreased with increasing immersion days. However, after 60 days of immersion, the passive current density decreased, increasing the protectiveness of the passive film [21]. Atomic fractions of FeCoCrMoSi AC coatings immersed in 3.5 wt.% NaCl solution for up to 60 days are shown in Fig. 3. Silicon was not detected due to its low content. The atomic mass of iron increased during immersion, the molybdenum content reduced, and the atomic mass of chromium remained stable. The author emphasizes that chromium and molybdenum played the main role of corrosion resistance. The amorphous structure proved to be effective for protection against corrosion in immersion tests, and the formation of a passive film with the immersion time occurred [21].

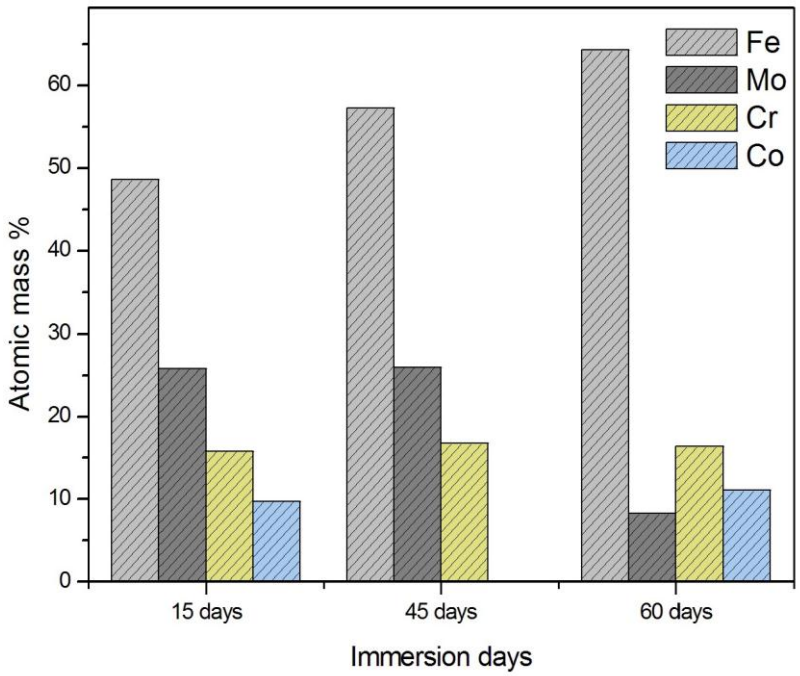

Figure 3. Atomic mass distribution of the FeCoCrMoSi AC coatings after up to 60 days in immersion in a saline solution

Karimi et al. [20] used image analysis techniques to evaluate the porosity, pore size and shape of the flame-sprayed NiCrBSi coatings before and after remelting processes. Temperatures of 950, 1000, 1050 and 1100 °C are used in the remelting processes. The remelting process decreased the porosity level (from 11.7 to 1.9%) and improved the metallurgical bonding between the carbon steel substrate and the coating. The pores in the as sprayed sample showed an irregular, elongated shape. More than 55% of pores were sharply disc shaped. After the remelting process, the pore shape was converted to a near spherical and non-flat spheroidal configuration [20]. Bergant et al. [25] analyzed the corrosion properties of flame-sprayed and heat-treated NiCrBSi on low-carbon steel. Bergantet al. [26] demonstrated that a post-treatment of annealing at 1080 ºC reduced the hysteresis loop in cyclic polarization curves and decreased the passive current densities of the flame-sprayed NiCrBSi coatings in an aqueous solution of 3.5 wt.% NaCl. The reduction of the hysteresis loop indicates a higher repassivation tendency, and the lower passive current density indicates the greater protective character of the passive layer. Bergant et al. [26] used a high temperature of partial remelting where almost complete fusion of the coatings occurs, which is close to that used by Karimi et al. [20]. They found that the heat treatment of the flame-sprayed coatings promotes densification and elimination of the porosity network, improving the corrosion resistance of the coatings.

Jamshidi et al. [27] studied the effect of the addition of Ti_3SiC_2 on the tribological and corrosion behavior of Al coatings. Oxy acetylene flame thermal sprayed coatings of aluminum matrix composites are used in the automotive industry on brake rotors, pistons, and connecting rods. The spraying distance, preheating of the substrate, and material feeding rate affected the sprayed coating properties. Torres et al. [28] reported that the decrease in spraying distance and the preheating of the substrate enhanced the adhesion between the substrate and coating. The hexagonal structure of Ti_3SiC_2 and the presence of silicon in its structure lead to the formation of a graphite-like layered structure. The corrosion current density of the Al coating, 1.417 mA cm^{-2}, is much higher than that of the composite coating, 0.532 mA cm^{-2}. Electrochemical impedance spectroscopy (EIS) analysis showed a higher corrosion resistance of the composite coatings in a saline medium than of the Al coating. However, the Al and the Al-Ti_3SiC_2 coatings showed passive behavior in the saline solution, and the passive current densities of the composite coatings are higher than those of the

aluminum coatings [27]. The introduction of a noble ceramic phase into the aluminum matrix increases the corrosion potential since the composite is nobler than pure aluminum. However, the composite has a higher porosity (5.2%) compared to the aluminum coating (2.1%). The increase in porosity and the heterogeneity produced by the addition of the Ti_3SiC_2 phase contribute to the increase in the passive current density, increasing the corrosion of the material.

Chen et al. [29] developed a flame-sprayed polymer/nano-Al_2O_3 coating with a tunable superhydrophilicity/superhydrophobicity achieved by changing the concentration of the polymer (polyurethane) in the starting suspension. The Al coatings were initially arc-sprayed onto steel substrates, followed by the deposition of polyurethane (PU)/nano-Al_2O_3 composites by a suspension flame spraying process. Large-scale corrosion-resistant superhydrophobic PU/nano-Al_2O_3-Al coatings were successfully fabricated. Suspension thermal spray is an exciting method suitable for fabricating nanostructured coatings due to its unique advantages of circumventing the preparation of micron-sized powder feedstock and retaining the chemistry of the nanostructured materials. The corrosion current density of the Al coating, 2.215×10^{-3} A.cm^{-2} is higher than the corrosion current density of the PU/nano-Al_2O_3 composite coating (1.873×10^{-4} A.cm^{-2}). The superior corrosion resistance of the PU/nano-Al_2O_3 coating is due to its super hydrophobic nature and the polyurethane addition that acts as an additional binder in the composite. From the polarization curves presented by Chen et al. [29] it is also possible to extract important information about the behavior against corrosion of the aluminum and PU/nano-Al_2O_3 coating, and the two coatings exhibit a passive behavior. In this way, the most important parameters in the evaluation of the corrosion resistance of materials are the passive current density and the breakdown potential. The composite coating showed the highest stability of the passive layer as the potential increased, as it showed the highest breakdown potential. And the passive layer of the composite coating showed the highest protective character with the lowest passive current density.

Shrestha and Sturgeon [30] verified the effectiveness of anti-corrosion coatings of 316L stainless steel (UNS S31603) and nickel alloy 625 (UNS N06625) applying coatings on a carbon steel base using commercial high velocity oxyfuel (HVOF) spraying systems and a high-velocity wire flame spraying system. The electrochemical behavior of the as-deposited materials was compared with the behavior of materials in their wrought form. The stainless steel and nickel alloy coatings produced using the high velocity wire flame spray system displayed a higher oxide volume compared with those produced using HVOF processes and a lower corrosion resistance. The authors estimated the amount of oxide present in the AISI 316L steel and nickel alloy 625 by using oxygen analysis, found 26 wt.% for the 316L coatings and 20 wt.% for the Ni alloy 625 coatings deposited by flame spraying. The nickel 625 and stainless steel 316L coatings made using the high velocity wire flame spray process present extensive oxidation, less adherence to the substrate, and corrosion resistance in saline solutions inferior to those produced with the HVOF process.

For biomedical applications, Mardali et al. [31] compared flame spraying to high velocity oxyfuel (HVOF) for hydroxyapatite depositions on magnesium alloy substrates. X-ray diffraction analysis showed that the volume of secondary phases in the HVOF deposited sample was less than that in the flame sprayed coatings. The elemental weight percentage of calcium in corroded surfaces was 21% and 34.5% for HVOF and flame-sprayed coatings, respectively. Contrary to the results of the EIS measurements for HVOF coating performed during the early hours of immersion in the simulated body fluid (SBF), flame-sprayed coating exhibited a lower corrosion rate after 5 h of immersion in the SBF solution. In the flame-sprayed samples, corrosion products formed a protective layer that increased corrosion resistance over time. The impedance at 0.1 Hz of the HVOF deposited hydroxyapatite on Mg alloy increased up to 600 Ω.cm^2 after 3 hours of immersion in SBF solution and thus decreased until 12 h of immersion, reaching 200 Ω.cm^2. The impedance at 0.1 Hz of the flame-sprayed hydroxyapatite on Mg alloy increased continuously reaching 850 Ω.cm^2 after 12 h of immersion in the SBF solution. And after 30 h of immersion in the HVOF solution, the flame-sprayed hydroxyapatite showed the lowest hydrogen evolution compared with the bare Mg alloy and the HVOF sprayed hydroxyapatite.

2.2. Atmospheric/ vacuum Plasma Spraying (APS/VPS)

The APS/VPS technique can present unfused particles, causing the appearance of cracks and pores. A representation of the atmospheric plasma spraying technique is shown in Fig. 4.

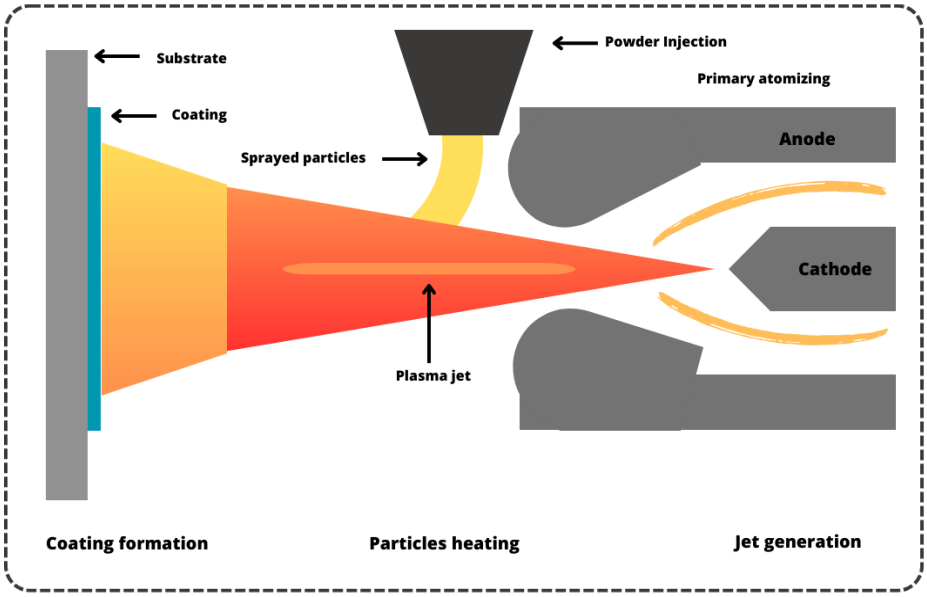

Figure 4. Scheme of the atmospheric plasma spraying technique

Considering that these problems are harmful to corrosion resistance, it is necessary to study the technique in more depth to produce coatings with adequate microstructural characteristics [32]. Kim et al. [32] studied the preparation of coatings with different powder particle sizes to produce an APS-Y_2O_3 coating that has good corrosion resistance. Reducing the size of the powder particles can reduce the defects in the coating and increase the bonding force between the melted powder particles [32].

Huang et al. [33] described the mechanism by which they elucidated the process by which the fluorine plasma attacked the coatings. During the first stage of corrosion, some regions showed the most severe etching: the fully melted region, non-fused particles, and pore edges. Many coating surface regions progressively fused and smoothened with the prolonged etching; in the meantime, the surface roughness decreased. On the surface coating were also formed corrosion products such as Al_2O_3, AlF_3, YOF and YF_3, and the etching product growth looked like the fungus Ganoderma lucidum; hence, the name 'fungal etching'. The focus of the study is to develop ceramic coatings resistant to corrosion by halogen plasma for application to semiconductor processing equipment.

Babu et al. [34] examined the electrochemical performance of atmospheric plasma spray $Cr3C_2$-NiCr-based coatings used as corrosion-resistant materials in the seal structures of gas turbines. The commercially available $75Cr_3C_2$–25NiCr (Metco 81NS) was used as a reference material and blended with B_4C and chromia (weight fractions of 5% and 10%) to improve the properties of the newly-developed plasma sprayed coatings. Open circuit potential and linear potentiodynamic polarization studies were carried out in artificial seawater to determine the electrochemical response and corrosion degradation mechanism of the plasma sprayed coatings. The corrosion resistance of the coatings strongly depended on the coating type, crack distribution, and porosity levels. The densification of the sample with the lowest corrosion current density was associated with minimal decomposition of the feedstock powder particles and the ability of Cr_2O_3 to form a reinforcement matrix. The peening effect of the harder and denser Cr_2O_3 particles during coating formation also improves the coating density. The presence of fewer interconnected cracks within the coating is responsible for reducing the diffusivity of chloride ions into the coating material. The decomposition of the B_4C particles during the plasma spray process adversely affects the electrochemical behavior of the as-sprayed coatings. The lower porosity and fewer interconnected cracks are the key factors enhancing the corrosion resistance of the composite-coated steel. The pores, cavities, and micro-cracks due to the quenching effect of the particle splats after deposition of the coating layer influenced the corrosion mechanism, allowing the corrosive agents to move through the coating layer, followed by the formation of corrosion products at the interfaces. The coating binder phase contained Ni, Cr, and chromia formed a continuous protective passivation film. With the increase in test duration, chloride ions reach the substrate. An accumulation of corrosion products

occurs at the coating/substrate interface, leading to coating failure and delamination.

Meghwal et al. [35] studied the corrosion performance in seawater of the AlCoCr0.5Ni high-entropy alloy coating developed by atmospheric plasma spray. The AlCoCr0.5Ni showed higher corrosion resistance in seawater than the AlCoCrFeNi HEA coating and the AISI 316L stainless steel. The atmospheric plasma AlCoCr0.5Ni sprayed coating presented a lower passive current density than the AISI 316L steel but also showed a lower breakdown potential in seawater. The passive layer of the AlCoCr0.5Ni coated steel seems to be more protective than the oxide layer of the AISI 316L, but the AISI 316L stainless steel showed a higher resistance to uniform corrosion, presenting a lower corrosion current density. This corrosion attack is triggered around coating defects, such as porosity, activating localized corrosion. The creation of superficial, sub-micron sized holes combined to form a mesh structure on the coating surface. The morphology of surface corrosion demonstrated a localized corrosive attack on the coating surface in the form of selective dissolution of Ni, Co, and Al. This behavior was attributed to preferential corrosion of the face-centered cubic (FCC) and ordered body centered cubic phases within the coating.

Another recent work by Guo et al. [36] presents a study on the improvement of corrosion resistance of AISI 316 steel by using a coating of ZrO_2 and TiO_2 deposited by air plasma sprayed technique in oxygenated sub- and supercritical water. In this work, the ceramic was sprayed through an air plasma spray plant on the dry substrate using a mixed gas made of argon and hydrogen with a flow ratio of 24:5. The coating exhibited a serrated morphology, and the ZrO_2 coating presented some small holes, which may be related to the material in the spray melting heterogeneously and causing aggregation of molten powder particles at the nozzle exit. The TiO_2 coating showed impure particles, which may be related to the existence of fine particles doped during the spraying process. Both coatings showed better corrosion protection than the substrate, but the TiO_2 coating showed a higher corrosion protection. It was still possible to see the need to deepen the research to optimize the air plasma spraying process to eliminate some defects, for example, pores, in the coating [36].

Hu et al. [37] studied the CeO_2/NiCoCrAlY composite coating, which provides a reliable and effective route to fabricate hydrophobic surfaces with applications in self-cleaning, antifog, anti-icing, and drag reduction. The APS technique was used due to its ability to obtain a surface morphology of single roughness on a double scale, which is beneficial to obtaining high hydrophobicity. In this study, a commercial APS system was used with NiCoCrAlY as raw material powders with various volume fractions of CeO_2, from 0% to 100%, using a mixture of argon and hydrogen gas; the substrate was placed 100 mm away from the jet nozzle. The coating has a thickness of ~200 µm, forming a rough structure with large islands randomly distributed; the large islands were formed by partially melted particles, and the small ones were formed by spatters of powders that were totally melted during the application of the coating. The hydrophobic coating showed a good ability to protect against corrosion (Table 1), being possible to apply in conditions of severe corrosive environments [37].

Table 1 – Electrochemical parameters of APS CeO_2/NiCoCrAlY coated steel

	Ecorr (V) $_{SCE}$	Icorr ($A.cm^{-2}$)
Steel substrate	-0.60	$8.1\ 10^{-5}$
20 v.% CeO_2/NiCoCrAlY coated steel	-0.47	$2.0\ 10^{-5}$
80 v.% CeO_2/NiCoCrAlY coated steel	-0.41	$3.0\ 10^{-6}$

Wang et al. [38] studied the corrosion behavior of the nickel-based superalloy substrate coated with calcium-magnesium-aluminum-silicate (CMAS) by air plasma spraying via burner equipment testing. Obtaining a ceramic coating with a thickness of 240 µm with different ceramics (8YSZ, 8YSZ + Y_2O_3, 38YSZ) was performed by APS, with the primary gas being argon and the secondary gas being hydrogen. The coating showed typical pores and microcracks; the 8YSZ + Y_2O_3 TBCs double layer coating showed CMAS corrosion resistance with practical properties [38].

To protect hot-section components, thermal barrier coatings (TBCs) are widely used in gas turbines and aircraft engines. Implementing TBCs, advanced aircraft service engines can withstand a temperature above the melting point of metallic parts, with improved thrust and weight matching and improved efficiency. With a layer of 200 to 400 µm of state-of-the-art TBCs, it allows decreasing the temperature of the superalloy substrate of the hot section components by approximately 100 °C. Conventional TBCs are composed of a thermally insulating ceramic coating and a metallic finish that resists oxidation. [39]. The most frequently used

deposition method for TBCs is atmospheric plasma spraying. Zhao et al. [39] investigated the oxidation performance of double-ceramic-layer thermal barrier coatings (DCL TBCs) deposited by atmospheric plasma spraying (APS) and suspension plasma spraying (SPS). Four varieties of APS-SPS DCL TBCs with dense/porous columnar structured or vertically cracked microstructures were made. The double-ceramic layer that was developed showed better oxidation resistance than the single-layer SPS TBC that was studied for comparison. The thermally grown oxide (TGO) in long-term oxidation can be divided into two layers, such as the outer mixed oxide layer and the inner alumina layer, in which the increasing rate of mixed oxide in the TGO changes during oxidation. In terms of oxidation lifetime, segmented APS-SPS TBCs showed slightly better performance than columnar APS-SPS TBCs. Among the four different APS-SPS TBCs, the segmented, dense APS-SPS TBCs with low vertical crack density seem to have more potential to be used for industrial applications [39].

Bakan and Vaßen [40] utilized the atmospheric plasma sprayed and various spray currents (275, 325, and 375 A) for Yb-silicate deposition on three different Si/Yb-silicate environmental barrier coating systems (EBCs). The EBCs were thermally cycled between room temperature and 1300 °C for up to 1000 h in air. Also, bare Si coatings were tested under isothermal and thermal cycling conditions in the as-sprayed state and after polishing at 1300 °C in air. It was observed that parabolic oxidation kinetics occurred; the spray conditions influenced the Yb-silicate which provided oxidation protection. Yb-silicate prevented the bond coat when a current of 375 A was used. The controlling mechanism occurs due to densification in the Yb-silicate layer during thermal cycling. The oxidation rate was also influenced by the surface finish of the Si coating. The TGO was thinner and less cracked on the polished APS Si coating in comparison with the as-sprayed Si coating surface.

An $Al_{0.5}$FeCoCrNiMn high-entropy alloy coating was deposited by using plasma spray on the surface of AISI 316 stainless steel [41]. The corrosion resistance of the coatings in 3.5 wt.% NaCl solution was evaluated and the coated steel exhibited a higher corrosion potential and a corrosion current density similar to that of AISI 316 steel [41]. As the immersion time increased, the charge transfer resistance of the coated steel increased, indicating an increasing corrosion resistance [41].

2.3. ARC spraying (ARC)

Arc spraying is a well-used technique for presenting high thermal efficiency, thermal impact, high spray efficiency, low cost, simple operation (Fig. 5), safety, and high coating thickness [42]. With the deposition of the coating on the substrate, a deformation occurs in lamellar structures, forming a coating with a heterogeneous structure. During the projection, oxidation can occur, which creates porosity and oxides in the intersplats in the coating [42]. This oxidation impairs the corrosion resistance of the coating [42], and it can be controlled with changes in spray parameters or changes in raw material [43].

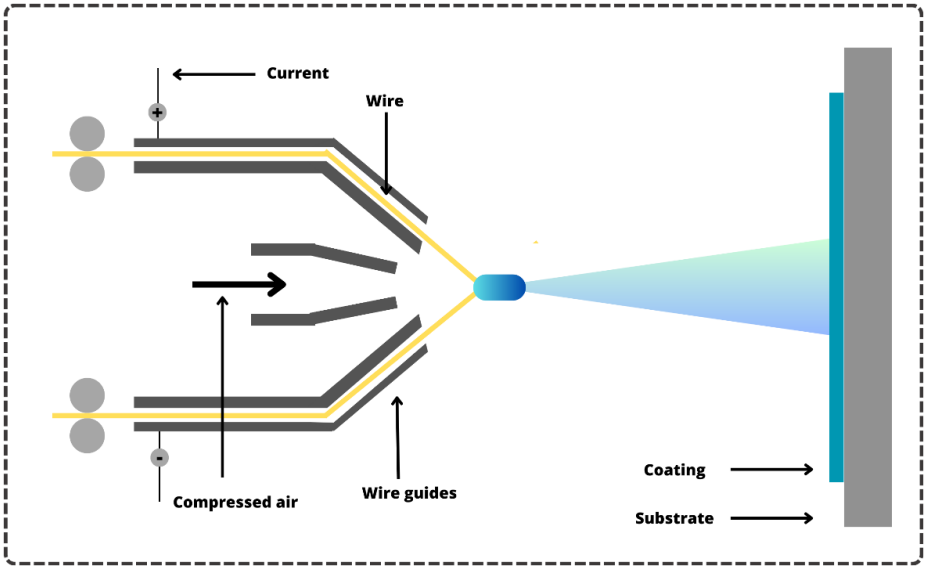

Figure 5. A scheme of the arc spraying technique

In view of this problem, Zhang et al. [42] studied the evolution of the microstructure and the corrosion properties induced by laser remelting of an Al-Fe-Nb-Ni coating consisting of some amorphous or nanocrystalline phase produced by ARC spraying. The coating was projected by a high-speed arc spraying system, in which tubular wire containing the coating powder was sprayed on the substrate (low carbon steel) at 200 mm obtaining a coating with a thickness of 500 μm, followed by a laser remelting process. A change in the structure of the phases before and after the laser refusion was observed, forming an amorphous or nanocrystalline structure. The coating after ARC was relatively dense and had a porosity of 2%. After laser refusion, the typical lamellar structures formed were eliminated, forming a densified and homogeneous coating. After remelting, the laser obtained an improvement in corrosion resistance compared to the coating without remelting [42].

Another form that has been used to decrease porosity is the application of sealants that fill the pores; however, annealing at the melting point of the coating can cause changes in the microstructure and stress relief [43]. An alternative is the use of water-soluble salt-inorganics for pore fillers. Singh et al. [43] carried out research studying the filling of the post-treatment pores of an Al coating deposited by the arc thermal sprinkler process and evaluating the corrosion of the coating. The deposition was performed with the substrate prepared 20 cm away from the pistol. The post-treatment to reduce porosity was performed with a nylon brush, dissolving different concentrations (0.1, 0.5, and 1 mol/L) of monobasic ammonium phosphate ($NH_4H_2PO_4$) and cesium nitrate ($CeNO_3$), whose contents were 0.001, 0.0025, and 0.005 mol/L. The three coatings obtained with these concentrations contained cesium aluminum oxide, $Ce_2Al_2O_3$, and ammonium aluminum hydrogen phosphate hydrate, $(NH_4)_3Al_5H_6(PO_4)_8.18H_2O$. The as-coated sample has defects and pores, which cause aggravation in the reduction of corrosion resistance; after the treatment, the pores and defects are filled, reducing the porosity of the coating from 47% up to 12% and improving the corrosion resistance of the material [43]. The coatings post-treated with 0.5 mol/L of monobasic ammonium phosphate and 0.0025 mol/L of cesium nitrate showed the highest impedance and corrosion resistance after 65 days of immersion in artificial seawater (Fig. 6). These coatings also showed the lowest anodic current densities in polarization curves obtained after 65 days of immersion in the artificial seawater. It is interesting to note the change in the corrosion mechanism of coatings, which presented a passivation zone in the as-deposited condition. However, the anodic current densities of the post-treated coatings increase continuously as the potential increases, indicating a change from a localized corrosion process to a uniform corrosion morphology.

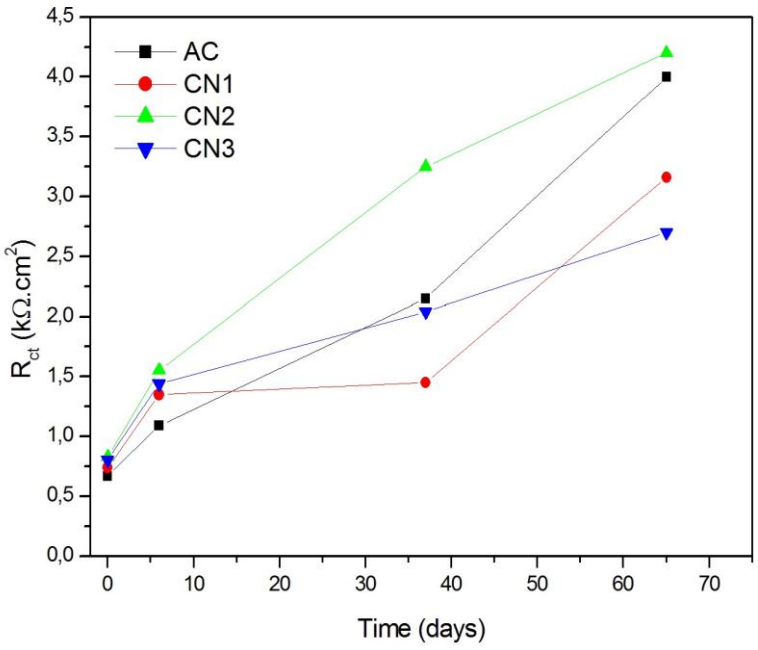

Figure 6. Charge transfer resistance of Al coatings deposited by using arc thermal sprinkler and post-treated in a solution of several concentrations of monobasic ammonium phosphate and cerium nitrate

Haixiang and Dejun [44] compared the electrochemical behavior of arc and laser thermal sprayed coatings on S355 structural steel, which is used in heavy engineering and ship building, in three electrolytes: 3.5% NaCl, 0.1 mol/L NaOH, and 0.1 mol/L sulfuric acid aqueous solutions. The morphology of the arc sprayed coating showed porosity, cracks, and oxide particles, with a roughness of ~6.073 μm. The porosity came from the semi–melted and unmelted Al particles, which were not completely connected; the cracks were attributed to the quenching stress after rapid cooling of molten aluminum; and the oxide particles came from the oxidation of aluminum particles at high temperature. The morphology of the laser thermal sprayed Al–Ti–Ni coating surface showed no obvious porosity or cracks, with a roughness of ~1.845 μm. The origins of Al, Ti, Ni, Fe, C and O elements in coatings were the same as those of arc-sprayed coating. The high Fe content was because of contraflow and mass transfer in the molten pool. The laser-thermal-sprayed coated steel showed a higher polarization resistance than the arc-thermal sprayed in the saline solution. However, the impedance of the coating was higher for the arc-thermal sprayed steel. In the acidic solution, the impedance modulus at lower frequencies of the substrate and the arc-thermal sprayed steel is close to zero, while the impedance modulus of the laser-thermal sprayed steel is 300 $\Omega.cm^2$. In the aqueous solution of sulfuric acid, the samples showed an inductive element, mainly the laser-thermal sprayed steel, indicating adsorbed species on the electrode. In the alkaline medium, the laser-thermal coated steel and the substrate differed, with the latter having a higher corrosion resistance than the arc-thermal sprayed steel. In a saline environment, the corrosion resistance of arc thermal-sprayed steel approached that of laser-thermal-sprayed steel.

2.4. Detonation gun spraying (DGS)

The detonation gun coating (DGS) method (Fig. 7) presents excellent adhesive force, low porosity, and compressive residual stresses on coating surfaces [45]. Some work has reported a good corrosion resistance of coatings produced by DGS in several media.

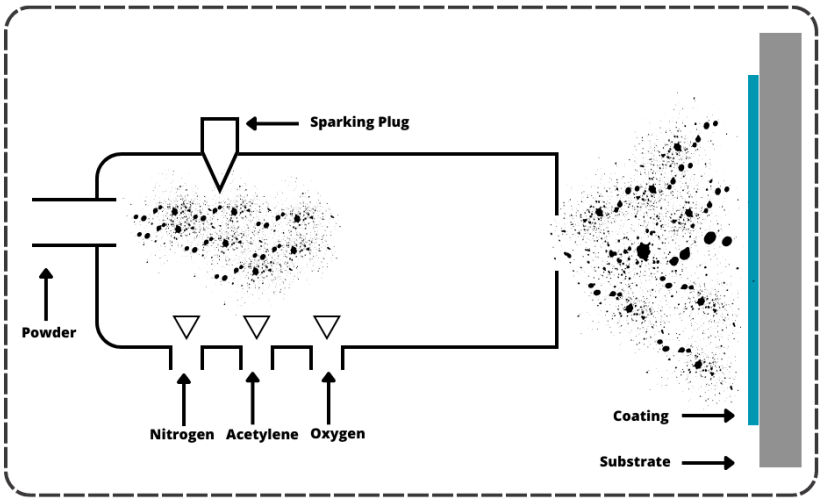

Figure 7. The detonation gun spraying method

Zhai et al. [46] published the study of corrosion in a 3.5% NaCl solution of an amorphous coating based on Fe on AZ31B magnesium alloy by detonation spray. Commercial Fe powder with a size of 15–55 μm was used, with spherical or almost spherical particles that were deposited on the substrate by detonation spray. The importance of the capacity for spoilage of the powder particles is due to ensuring good fluidity for the functionality of the method. Both the powder and the coating have an amorphous structure. The presence of an amorphous coating is given by the ability of the powder to form glass and the high flight speed of the particles, in addition to the influence of the restraining rate of the DGS. The structure obtained does not present spatter phenomena, demonstrating the level of gun

spraying detonation technology to produce amorphous structures based on Fe. Due to the disordered structure of the coating, the density provides for the formation of a passive film that improves corrosion resistance on the studied substrate [46].

The technique has also been applied for hot corrosion protection. The high-temperature corrosion of boiler parts, such as water walls and superheated tubes, impaired the efficiency of thermal power plants. Kumar et al. [47] analyzed the behavior of diverse thermal spray processes deposited on distinct coatings and reported the best coatings to prevent hot corrosion of boiler tubes.

Kamal et al. [45] studied the influence of Cr_3C_2-NiCr coating on the hot corrosion behavior of Ni and Fe-based superalloys. A powder with irregular morphology between 36.10 µm and 9.3 µm was sprayed on the substrate with standard parameters. The coating obtained presents a flat splat microstructure with uniform fine grain, low porosity, good adhesion, and a film thickness of 200–250 µm. It attributes a better resistance to hot corrosion to the coating compared to uncoated samples [45].

Talako et al. [48] analyzed the structure and properties of detonation gun sprayed (DS) coatings from the powder that was synthesized based on FeAlSi/Al2O3. FeAl-based coatings are protective in different environments, like corrosive, oxidizing, carburizing, and sulfurizing ones.

High-quality coatings with a porosity less than 1 vol% and a nanocomposite structure were obtained from the synthesized powder using a computer-aided 'Perun-S' detonation gun complex. As-sprayed coatings from the synthesized FeAlSi/alumina powder demonstrated a high temperature erosion resistance. Oxide dominated erosion with mixed brittle-ductile wear behavior is more likely to occur in the coatings at 550 °C. The main reasons for the slower oxidation kinetics of the FeAlSi/alumina coatings are the promotion of alumina formation during oxidation and the reduction in Fe_2O_3 concentration in the oxide scale when compared with those of the basic Fe-Al eutectoid composition.

2.5. Cold Sprayed (CS)

In the mid-1980s, the Papyrin research group invented the cold spray process in Russia. The primary components of the cold spray system with spraying segment are a supersonic nozzle, powder hopper, and gas heating coil (Fig. 8). In the cold spray process, high- pressure processing gases such as helium or nitrogen are used. Powder in the feed stock is heated below the melting temperature of the powder, and it passes through the supersonic nozzle (de Laval nozzle) with high velocity, impinging on the substrate. The coating is produced under a plastically deformed condition with low porosity and high adhesion and cohesion strength, which ameliorates the hardness, corrosion, and wear resistance of the coatings [49,50].

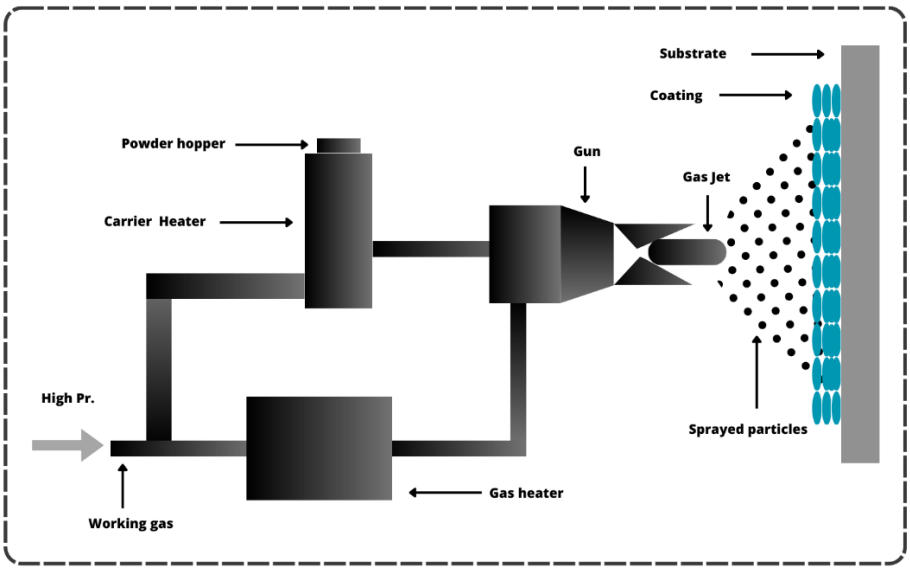

Figure 8. A scheme of the cold spraying technique

The cold spray process has a clean manufacturing environment without burning fossil fuel; the coating is formed under low-temperature heating of powder with high velocity impingement on the substrate. Cold-sprayed coatings usually showed good hardness, scratch resistance, and corrosion resistance for all types of applications in the aerospace, marine, and automobile industries [3].

Cold spray is an advanced and effective additive manufacturing method. In the cold spray techniques, the metallic or alloyed particles are stimulated through a stream of supersonic gas flow and then deposited onto a substrate under a certain pressure and temperature (Fig. 6). The sprayed particles often experience significant plastic deformation compared to traditional thermal spray techniques. The oxidation, phase transition, and thermal stresses can be reduced because initially the powder particles remain in the solid state throughout the cold spray deposition. CS can be used to deposit different pure metals and their alloys. CS has been applied to convalesce the surface functionalization of parts used in various fields for providing adequate protection against high temperature corrosion, oxidation, and chemical reactions [4]. The key distinction from other methods is that cold spraying uses kinetic energy instead of thermal energy for particle deposition, and the processing temperature is often held below the melting temperature of the powder particle [5]. While several numerical simulations and experimental analyses were carried out to learn about the mechanics of bonding in cold spray, they were not properly understood [6]. At present, adiabatic shear instability is correlated with the most probable bonding mechanism for the cold spray process [7]. In this mechanics, bonding criteria are formed between particle–particle (cohesion strength of 30–100 MPa) and particle–substrate (adhesion strength of 30–120 MPa) during impact; areas undergo extreme localized shear deformation that interrupts the thin oxide films, allowing intense particle–substrate contact [8]. In this method, the temperature will be below 800 °C, whereas in other thermal spraying techniques, the temperature will be beyond 2000 °C. On the other side, the impingement velocity of the powder particles on the substrate is around 1200 m/s. It is also possible to deposit extremely dense and heavy coatings with a thickness of 100 µm to 1500 µm by using cold spray techniques [49].

The cold spray technique has been used in the production of coatings with good corrosion resistance. This technique has been widely used because it presents few problems, such as oxidation and thermal stresses, which are avoided due to the low temperature used in the process.

Bai et al. [51] analyzed the corrosion performance of Al-Al_2O_3 cold sprayed coatings on mild carbon steel pipe under thermal insulation. The obtained results showed that with the addition of α-Al_2O_3 in spraying powder, the coating gets a higher hardness and denser microstructure. From corrosion under insulation (CUI) tests, Al-Al_2O_3 coatings were efficient in protecting carbon steel pipe from CUI due to the lamellar microstructures of the coatings. When these coatings were exposed to higher concentrations of NaCl, they exhibited faster degradation [51].

Whitharamage et al. [52] also reported metallic coatings for aluminum alloys by cold spray technique. The results were obtained by X-ray spectroscopy, scanning and transmission electron microscope (SEM/TEM), X-ray diffraction, electrochemical impedance spectroscopy, potentiodynamic polarization tests, immersion tests, and resistance ammeter tests. The cold-sprayed alloy exhibited low corrosion current density and a clear passive window with a high pitting potential in an aqueous solution of 0.01 M NaCl (Table 2). The cold-sprayed alloy showed higher film impedance and charge transfer resistance than the Al alloy (Table 2). This high corrosion resistance has been attributed to the nanocrystalline structure and high solid solubility of vanadium in aluminum. Since Al-M alloys are in a metastable state, CS could retain high solid solubility and grain refinements in the coating, which is expected to result in highly corrosion-resistant coatings. The cold sprayed coating and the substrate had excellent galvanic compatibility. Zero-resistance ammeter (ZRA) tests showed that the coating acts as a sacrificial anode to the substrate, indicating its ability to protect the substrate from corrosion in the event of coating breakdown. Cold-sprayed coatings of ball-milled alloys could be applied to a wide range of Al alloys, which can expand the application of high-strength Al alloys in harsh environments. Moreover, the composition and microstructure of the coatings vary according to the electrochemical properties of the substrate [52]. The occasional discontinuity in coatings, such as crevice formation during cold spray, facilitates electrolyte penetration toward the coating-substrate interface. Once the electrolyte has reached the coating/substrate interface, localized corrosion is favored due to the galvanic interaction between the coating and substrate, which acts as a cathode. The coating releases Al and V ions. The released vanadium ions could inhibit corrosion at the coating/substrate interface. The inhibition mechanism could be like that reported for vanadates. This hypothesis of vanadium release on

repassivation for the cold-sprayed alloys needs to be validated in future studies. Nonetheless, the deposition of V on cathodic iron and carbon-rich particles in Al-V alloys resulting in high corrosion resistance has been shown by Chirstudasjustus et al. [53] and Witharamage et al. [54] by analyzing the pits using scanning transmission electron microscopy.

Table 2 – Electrochemical parameters of cold spray coating and AA2024-T3 aluminum alloy

	CS-Al-5V	AA2024-T3
Ecorr (mV_{SCE})	-491±29	-465±5
icorr ($\mu A.cm^{-2}$)	0.02±0.01	0.86±0.12
Epit (mV_{SCE})	-407±20	-
Rfilm ($k\Omega.cm^2$)	921	73
Rct ($k\Omega.cm^2$)	1026	166

The characteristics of the powder used in the production of the coating have a great influence on the quality and properties of the coating. Chu et al. [55] used a hard spherical, an angular, and a soft spherical tantalum powder and a mixture of tantalum powders to produce a coating. Using cold spraying, the work showed that these characteristics and powder mixtures have effects on the porosity, cohesive strength, and corrosion resistance properties of the coating [55]. The angular tantalum generates the highest deposition efficiency, corrosion resistance, and tensile strength, mainly due to its highest impact velocity, and the angular morphology facilitates both mechanical and metallurgical bond formation. For the two spherical powders, no evident metallurgical bonding is observed in the coatings, and the soft powder with reduced powder oxygen content exhibits a larger particle flattening ratio and leads to better tensile strength and corrosion resistance than the hard powder due to stronger mechanical interlocking. The soft powder promoted more particle bulk deformation but could not effectively facilitate the deposition of tantalum. The mixture of the angular with the hard powder increased both mechanical anchorage sites and metallurgical bonding components (due to localized stress concentration and disruption of surface oxides). Creating a hardness difference among feedstocks (a mixture of hard and soft powder) is beneficial to generate higher levels of strain at the soft particle side to initiate the formation of metallurgical bonding upon impact [55].

Understanding the powder adhesion mechanism in cold spray is primordial to controlling coating formation. Previous studies have suggested that metallic coatings are governed by metallurgical bonding, but no consensus has been established regarding the bonding mechanisms of ceramic particles. Zhou et al. [56] investigated the deposition mechanism of agglomerated gallium nitride (GaN) particles cold sprayed on stainless steel substrates. The evolution of the oxide layer thickness and coating-particle microstructures was analyzed by X-ray photoelectron spectroscopy and transmission electron microscopy. The results revealed that although mechanical interlocking and coating thickness were enhanced by the substrate surface roughness, grain refinement was not the key factor for the brittle particle deposition, considering the diameter of the nano-sized particles. Before cold spray, the original oxide layer thickness of the feedstock powder is rather insignificant, and the stainless-steel substrate surface exhibits a 12.10 nm thick oxide layer. Instead, a new interfacial oxide layer was formed because of the destruction and removal of native oxide films upon impact. A new oxide layer, around 18.14 nm thick, is formed at the coating/substrate interface, proven to be Ga_2O_3. Local heteroepitaxy between the GaN and stainless steel was observed and is regarded as a critical factor that promotes the adhesion of the coatings.

Luo et al. [57] deposited high purity aluminum (Al) and AlMgSi alloy coatings on Mg alloys by using an in-situ micro-forging (MF) assisted cold spray (MFCS) process for simultaneous higher corrosion resistance and a longer fatigue lifetime. In in-situ micro-forging assisted cold spraying (MFCS), large-sized shot peening particles are injected onto the coated layer at the same time as coating spraying, so the coated layer could be in-situ forged and densified by the shot peening particle. Dense metallic coatings could be prepared at a lower gas consumption rate, and the shot-peening particles sprayed out could be connected by an electromagnet and reused. Therefore, the MFCS process is more economical than conventional cold spray, in which high pressure gas (up to 5 MPa) or helium gas is needed to prepare coatings with low porosity. The in-situ MF contributes to a dense microstructure, refines the grain of the deposited Al alloy coating to the sub-micrometer range due to enhanced dynamic recrystallization, and generates notable compressive residual stress up to 210 MPa within the AlMgSi coating. The absence of secondary phases in the AlMgSi alloy coatings improves the corrosion resistance of the coated Mg alloy, which is even better than its bulk AlMgSi counterparts. The unique combination of refined microstructure and the prominent compressive residual stress within the AlMgSi coatings delayed the crack initiation upon repeated dynamic loading, increasing the fatigue lifetime of the Mg alloy. But this beneficial effect of increased fatigue strength is not observed for

aluminum coatings on Mg alloys, due to the low mechanical strength of aluminum.

Daroonparvar et al. [58] coated the cold sprayed aluminum AZ31B Mg alloy with cold sprayed Ti and Ta/Ti coatings, which noticeably reduced the wear rate of the Al coated Mg alloy. They reported that the high surface activity of commercially pure Al coating, diffusion-controlled reactions, and formation of corrosion pits could be mitigated using Ti top coating. However, a dense layer of Ta on the Ti coating exceptionally improved the corrosion resistance of the Ti/Al coated AZ31B Mg alloy in a neutral 3.5 wt.% NaCl solution. This work presents a new strategy to considerably raise the wear and corrosion resistances of cold spray Al coated Mg alloys by using double layered Ta/Ti coatings.

Norrell et al. [59] investigated the synergistic and individual effects of nano boron carbide (nB4C) and boron nitride nanoplatelets (BNNP) on the corrosion behavior of cold-spray aluminum matrix composite (MMC) coatings. Four novel Al MMC coatings with reinforcements were studied, consisting of either 2 vol.% nB4C, 2 vol.% BNNP, or dual nanoparticle reinforcement consisting of 1 vol.% nB4C plus 1 vol.% BNNP. Coatings were subjected to 500 h and 2000 h corrosion tests in a salt fog chamber consisting of 3.5% NaCl to simulate an aggressive marine environment. Following 500 h corrosion testing, each composite coating experienced mild to severe pitting throughout a significant portion of the coating. Following 2000 h of exposure, in addition to severe pitting, all coatings experienced galvanic corrosion at the coating/substrate interface.

Wei et al. [60] also used the technique reported by Luo et al. [56] to study micro-forging cold spray to spray three nickel powders: spherical gas-atomized Ni (GA-Ni), carbonyl irregular Ni (C-Ni), and electrolytic dendritic porous Ni (E-Ni) on magnesium alloys. Even though all deposited coatings present low porosity, the C-Ni and E-Ni coatings show poorer inter-particle bonding than the GA-Ni coating. Electrochemical tests show that the inter-particle gaps will act as fast ways for the corrosive media to penetrate the coatings; therefore, the GA-Ni coating, with intimate inter-particle boundaries, isolates the corrosive media for 3000 h and the C-Ni and E-Ni coatings fail after less than 10 h of corrosion.

Despite being a relatively new technique, cold spray has been widely applied in many engineering disciplines and applications, such as hydropower [61], military helicopters [62], manufacturing mold component repairs [63], and additive manufacturing [64]. The primary functions and advantages of CS coatings are to enhance wear [65, 66], erosion [61], fatigue [67, 68], and corrosion resistance [69, 70]. Cold spraying finds applications in corrosion protection and in the electrical and thermal fields, where the absence of oxidation may offer improved conductivity for materials [71]. Aluminum and aluminum alloy cold sprayed coatings are being investigated for repair/refurbishment of space shuttle solid rocket boosters and others (aerospace), repair and retrieval of parts and plate stocks used in aircraft structures (aircraft industry), repair/refurbishment of casings (gas turbine), and corrosion protection coatings (petrochemicals) [71]. High-performance layers such as high temperature oxidation resistant MCrAlY coatings, high conductivity copper/silver coatings, and phase-pure biocoatings are produced in vacuum plasma spray systems or physical vapor deposition systems. These systems are extremely expensive to both install and operate. Moreover, the cold-spray process may lend itself to collecting the overspray and reprocessing these expensive raw materials. Hence, well-founded cold spray technology will be able to compete for a good market share of VPS/PVD coatings in turbine, power, electronic/electrical, biotechnology, and other industries [71]. Cold spray has encompassed the medical field and has been used to deposit hydroxyapatite (HAP), a well-known biocompatible material, on several substrates without compromising the integrity of HAP [71].

The cold spray deposition of Inconel using air as a process gas is not only interesting from an academic point of view but also has implications for industry. In addition to this, the high velocity impact of Inconel feedstock severely deforms the microstructure in the deformed coatings, which has a direct influence on the functionality of the coatings. For instance, microstructural alteration due to hot deformation, such as the evolution of twins and the conversion of dislocation cells into low-angle and high angle grain boundaries, has a strong influence on the mechanical properties and electrochemical corrosion performance of nickel-based materials. Thus, Devi et al. [72] deposited IN625 and IN718 onto grit blasted Al-2024 substrates using air as a process gas at different process temperatures at a constant 20 bar stagnation pressure. The coating's inter-splat bonding state was characterized by microstructural, mechanical, and electrochemical studies. The polarization curves of IN625 showed passive regions in an aqueous solution of 3.5 wt.% NaCl, and the breakdown potentials of coatings deposited at 600 ^{o}C and 700 ^{o}C were the lowest. The IN718 coatings deposited at 650 ^{o}C showed the lowest breakdown potential, indicating premature degradation of the passive layer. The EIS measurements indicated that the bulk

and the 800 ºC stagnation temperature coatings of IN625 and IN718 showed the highest impedance and the highest corrosion resistance in a saline solution. The coatings, deposited at 800 °C, exhibit a lower fraction of low angle grain boundaries, which affected the corrosion resistance of the samples.

Tripathy et al. [73] produced corrosion resistant nickel coatings on preheated mild steel substrates by cold spraying. The substrate deposition temperature was varied, and post-fabrication annealing was introduced to reduce the deposition impact stress. Post deposition heat treatment, although improving interfacial bonding, leads to increased corrosion due to the porosity of the samples. Coatings deposited at low temperatures (~500 °C) provide the highest corrosion resistance, as evidenced by their microstructure.

While a high percentage of coating porosity is generally detrimental to the material's corrosion behavior, a porous coating for biomaterials enhances the biological response for bone fixation. The adhesion and cohesion strengths of porous coatings can be improved by adjusting the porosity levels of the coating system. Wathanyu et al. [74] studied the corrosion resistance and biocompatibility of a titanium (Ti) porous coating with high and low porosity gradients on grit-blasted and ground 316L stainless steel by cold spray. The coatings comprised a low porosity layer (the 1st layer) at the interface coating/substrate and higher porosity layers (the 2nd and 3rd layers) on top. The high and low porosity gradient samples had 8 % and 1 % porosity gradients, respectively. They related to the differing porosity between the 2nd and 3rd layers, deposited by the different process gas pressure used for the 2nd layer. All EIS results presented capacitive behavior (high corrosion resistance) with a phase angle close to −90°. High polarization resistance in the ground substrate indicated a highly stable passive film at the interface of coating/substrate, which was higher than the grit-blasted substrate. Surface preparation with grinding also exhibited a lower corrosion rate than grit blasting. SEM morphologies of the Ti/grit-blasted and Ti/ground substrates showed cracks in the embedded alumina and coating for the grit-blasted substrate and a non-continuous gap for the ground substrate. However, the high and low porosity gradients affected the EIS result and corrosion rate. The rough surface provided by the grit blasted substrate had lower charge transfer resistance values than those of the ground surface substrate. After 21 days of immersion in the saline solution, the porosity gradient did not affect the charge transfer resistance values for the grit blasted substrate. However, the lower porosity gradient of the coating increased the corrosion resistance of the sample where the substrate was ground. Porous structures in all Ti coatings could promote bone cell ingrowth.

From a corrosion perspective, CS SS coatings produced with helium (as process gas) show higher corrosion resistance than coatings deposited with nitrogen propellant gas in 3.5 wt. % NaCl solution. This was partially related to the porosity level reduction from 6.3% (for 316 L-N_2 coating) to 4.9% (for 316 L-He coating) as well as the enhancement of particle-particle bonding at inter-particle boundaries. Helium gas, with its lower molecular weight and higher thermal expansion coefficient, can easily reach higher velocities compared to nitrogen process gas at the same gas temperatures. However, due to the high cost of helium and its limited availability, this gas should be replaced with other cheaper and more accessible processing gases, such as nitrogen. On the other hand, the 316L powders due to their high strength are hard to plastically deform upon their impacts during the cold-spraying process. So, high porosity levels and relatively poor inter-particle bonding are expected in as-sprayed 316 L coating/deposits (especially when nitrogen is used as a process gas). This can adversely affect their properties compared to their wrought counterparts.

Yin et al. [75] cold-sprayed spherical 316 L powder particles using nitrogen process gas with an inlet pressure of 3.0 MPa and a temperature of 1000 °C. They were able to produce 316 L deposits with a porosity level of about 2.5%−4.3%. Hence, the production of 316 L deposits/coatings with lower relative porosity levels will be achievable using HPCS systems and process optimization when nitrogen is used as a propellant gas. Ralls et al. [76] produced a 316L coating on a wrought 316L steel substrate by using high-pressure cold spray. The microstructure of the CS coating was refined compared with the bulk sample and contains micropores at the interparticle boundaries. EIS and PDP tests demonstrated that the bulk sample had a relatively lower corrosion rate than the CS sample. In fact, the high density of dislocations in the CS sample is accountable for the lower anticorrosion performance compared to the bulk 316 L sample. Interestingly, the re-passivation ability of the CS coating was better than that of the bulk sample. This is due to the stored energy in the as-sprayed sample. This has made the re-passivation easier for the CS 316 L sample compared to the bulk sample in chloride-containing solutions.

Zhu et al. [77] worked with a cold spray made with a dense CoCrFeNi high entropy alloys (HEAs) coating with homogeneous microstructure on AZ91 alloy. Innovatively, the HEAs were cross-integrated with Mg alloys, utilizing cold spray to

break through the "bottleneck" of Mg alloys. The coating showed considerable spontaneous passivation caused by the multi-layer passive film composed of FeO, Cr_2O_3, and NiO. After 28 days of immersion in an aqueous solution of 3.5 wt.% NaCl, the weight loss of CoCrFeNi coated AZ91 plates was below 1%. The formation of large pits was restricted; however, lots of tiny micro-pits in sizes less than 1 μm were distributed on the corroded coating surface. The fast initiations of new pits were triggered by the repeatedly repassivation effect and the competing effect. The decrease in corrosion rate was caused by the stable passive film and uniform microstructure of the coating. In the Bode diagram, the impedance modulus of the CoCrFeNi coated AZ91alloy was at least three orders of magnitude greater than that of the bare Mg alloy. The bare Mg alloy exhibited a maximum at 200 Hz at an angle of 50 degrees, while the CoCrFeNi coated Mg alloy exhibited a wider maximum, at an angle of 70 degrees, indicating a more capacitive behavior and more corrosion resistance in saline environments. The polarization curve of the coated sample was shifted towards higher potentials and lower current densities, moving from a generalized corrosion mechanism to a passivation mechanism, with a pitting potential of 813 mV (SCE). The shielding reaction of the coating can enhance the surface protection of magnesium alloys.

To improve the corrosion resistance of Mg alloy, Yao et al. [78] produced a Zn coating by cold spraying technology and by post shot-peening processing. Mg alloys after machining showed lower corrosion current densities and corrosion rates due to decreased surface roughness. However, the anodic current densities were lowest for the Zn coated Mg alloy without shot peening. The shot peening can induce additional surface defects that could potentially accelerate the corrosion, but it also promotes the anti-corrosion characteristic induced by the improved surface microstructure with dense surface layers in shot-peened Zn coatings. Therefore, the increase in corrosion resistance (lowest corrosion rate) of shot-peened Zn coatings was mainly attributed to the formation of a dense surface layer with low roughness.

Owing to its low temperatures, the cold spray process is a new alternative method for spraying nanostructured materials [71]. As an advantage in cold spray there is no particle melting, and all the nanostructure is kept intact during the process.

Wang et al. [79] improved the corrosion resistance of cold sprayed zinc (CSZ) coating by adding graphene oxide (GO). To increase the degree of GO distribution in the CSZ coating, a SiO2-GOhybrid was formed, improving the hydrophobic performance of the coating. The SiO_2-GO in the CSZ coating provides excellent dispersion. The composite coating showed low surface energy and a hydrophobic effect, and the contact angle reached 125.78°. In contrast to the GO/CSZ coating, the tensile adhesion of the SiO2-GO/CSZ coating was substantially improved, reaching 0.7 MPa. The Tafel polarization curve and the electrochemical impedance test demonstrated that the addition of 0.4% by weight of SiO2-GO in the composition increased the barrier time and the cathodic protection cycle of the CSZ coating under the finish protection. The preliminary corrosion resistance of 0.4 wt% SiO2-GO/CSZ improved by 24%. The coating showed good coating structure and corrosion resistance after 50 days of immersion in a 3.5 wt.% NaCl solution.

A Zn-Al cathodic protection coating is great for adding corrosion protection to carbon steel. Yet, under seawater, erosion will encourage an increased speed of abrasion in low hardness coatings. Improvement of anti-wear properties of Zn-Al coating in seawater, self-lubricating Zn-xrGO/Al composite coatings (x is composition of rGO in Al powders = 0.1 wt.%, 0.2 wt.%, 0.3 wt.%) were deposited on low carbon steel by means of a low pressure cold sputtering method by Wu et al. [79]. A 20% increase in hardness of the Zn-Al coating is observed in contrast to the rGO coating with an Al concentration of 0.2 wt.% and the Zn-0.2 wt.% of the rGO/Al coating. The Zn-0.2wt% rGO/Al coating showed better self-lubrication properties with the usual generation of a lubrication platform with a low COF value of 0.22 when used in NaCl saline solution. The synergetic action of the frictional heat and the anodic polarization effect provided by the high electronegativity rGO leads to the formation of a lubrication platform that promotes the creation of a layer of materials resulting from corrosion, compensating for the consumption of the lubricating film. Zn coatings were used on substrates of carbon steel and on Mg alloys, two materials with low corrosion resistance in several media. Xie et al. [81] deposited pure Zn coatings on AZ31b substrates by cold spraying. The results indicated that the dense, low-porosity Zn coatings were successfully deposited on AZ31b magnesium with good mechanical properties. The cold sprayed pure Zn coatings exhibited higher corrosion resistance than that of the substrate, and the open circuit potential and corrosion potential of the cold-sprayed Zn coatings were close to those of bulk Zn. A change involving the diffusion of reactants and production through corrosion products in the EIS equivalent circuit was observed during immersion for 10 d. The corrosion behavior was related to the unique morphology of the cold-

sprayed Zn coating, and a "corrosion tunnel" was observed in the cross-section of the coatings after immersion, corresponding to the evolutionary mechanism of the particle–particle interface microstructure.

Koivuluoto and Vuoristo [82] highlighted that cold-sprayed coatings with impermeable structures have high potential to be used in the corrosion protection of metals and alloys. Denseness improvement can be achieved by optimizing the powder feedstock, adding hard particles to the metallic powder, and by laser assistance and a post-heat treatment. A dense coating requires a high level of plastic deformation, adiabatic shear instability conditions on the impact, and material jet formation [82]. Dense and low porous coatings were produced by using cold spraying from metallic powder feedstocks such as Al, Zn, Cu, Ti, Ta, stainless steel, Ni, and Ni alloys [82].

2.6. HVOF, HVAF and LVOF techniques

The HVOF technique (Fig. 9) presents extremely high particle speed and a comparatively low flame temperature with other spraying hot ranges, besides presenting higher strength of support, lower oxide content, and denser structure [83].

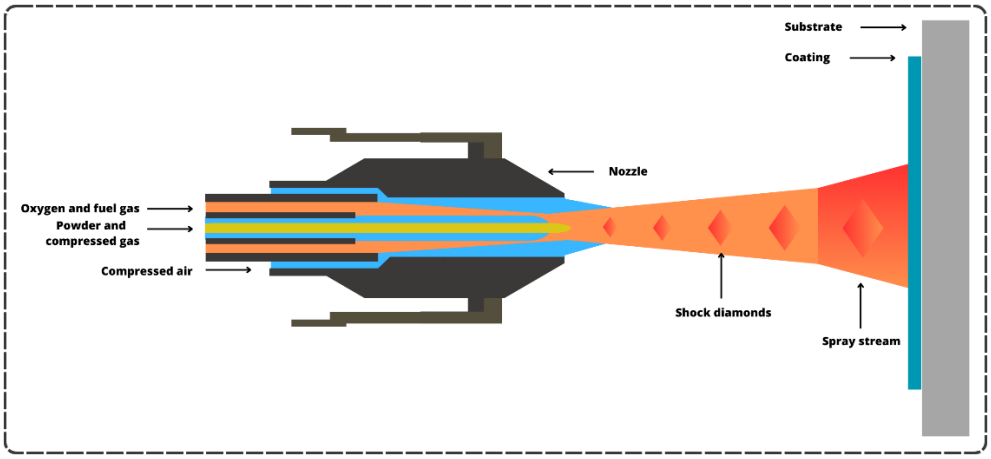

Figure 9. A scheme of the high velocity oxy fuel technique

Bhushan et al. [84] discussed the passivation tendency and corrosion resistance of a novel Fe66.59C11.70P7.58Mn0.37Si2.86Cr1.72Mo0.92B 8.26 amorphous coating prepared from pig-iron deposited on mild steel using a high-velocity oxy-fuel (HVOF) thermal spray process. At a lower Cr level, it was possible to achieve passivity within a short period of exposure to a corrosive environment. The coatings have been prepared from water-atomized feedstock powder, which is compositionally modified high-phosphorous pig iron melt and deposited using the HVOF spray technique under variable powder feed rates on mild steel (MS). The thinner coatings (150 µm), with lower porosity (1-3%), showed better behavior against corrosion in a saline environment. As the feed rate increased, there was an increase in the impedance of the coated steel. After 30 days of exposure to the salt spray test, the coated steel produced at the lowest feed rate of 25 g/min. and thickness of 300 µm showed the highest corrosion rate. The spectroscopic analysis of corroded samples reveals the formation of films of iron chromate and phosphates and protective iron-based rust phases on all the coatings.

Wang et al. [85] studied the long-term corrosion behavior of HVOF sprayed Cr_3C_2-NiCr coatings in a 3.5% NaCl solution containing sulfide. The coating is composed of two phases, one being the Ni-Cr phase, which has a high corrosion resistance and serves as a linkage for chromium carbide particles, and another containing chromium carbide, which mainly confers excellent wear resistance. The use of HVOF is due to its capacity to produce coatings with a high density and superior corrosion resistance. Post-spherical Cr_3C_2-NiCr particles were used, which can allow for better fluidity when compared to particles with an irregular shape. The coating was dense, with a thickness of about 350 µm, and an imperceptible layered structure. The coating showed the same behavior as a general tendency to increase first and then decrease the corrosion rate in different solutions during immersion testing [85].

Nickel-based self-fluxing thermally sprayed alloys have been used in many applications to protect machinery parts against wear and

corrosion. Gil et al. [86] produced a NiWCrBSiC coating on an ASTM 1020 carbon steel by using the HVOF technique. The authors focused on the microstructural characterization of coatings and found a well distributed network of hard phases. They found borides such as Cr_5B_3, Cr1.8W3.2 B3, $W_5(B,Si)_3$, B305Si8.44 and B_4Si), carbides (including $M_{23}C_6$, where metals (M) are Cr, W, Si, and Ni), silicon carbide (C0.17Fe0.81Si0.02), tungsten carbide (W3C), silicide (Ni_2Si), and trimetallics (Ni2.9Cr0.7Fe0.36). In particular, the existence of the borides had not been reported in the literature before, possibly owing to their small size, of 0. 31 μm.

Cheng et al. [83] optimized HVOF parameters to produce a CuAlNiTiSi mid-entropy alloy (MEA) coating and analyzed the microstructure and corrosion behavior. The parameters were optimized considering the reduction of coating porosity. The study showed that there is an interaction effect between three spray parameters on the porosity of the coating, and the oxygen flow has the greatest influence on the porosity of the coating. The optimized condition coating was dense and exhibited a single phase of solid body-centered cube (BCC) solution. The corrosion study demonstrated a porosity reduction effect to improve coating corrosion resistance. We can observe the influence of the optimization of the parameters through the electrochemical tests of potentiodynamic polarization and EIS measurements, in which the coating carried out with the optimized parameters presents better corrosion resistance than other coatings carried out under other conditions (Table 3). The process parameters of the non-optimized condition shown in Table 3 are the oxygen flow of 873.1 L/min, the kerosene flow of 0.42 L/min, and a spray distance of 320 mm. The optimized condition for HVOF spraying consists of a spray distance of 320 mm, and oxygen and kerosene flow of 802.3 L/min and 0.38 L/min, respectively. The Nyquist plot will show the optimized sample has a larger semicircle diameter, than the other samples, and the larger the semicircle diameter, the better the corrosion resistance. The Bode plot indicates that the optimized coating has a higher impedance value at low frequencies and a higher phase angle at its maximum at a middle frequency. The optimized coating showed excellent corrosion resistance in a medium of 3.5 wt.% NaCl solution, attributed to its low porosity and single-phase structure [83].

Table 3- Electrochemical parameters of a non-optimized coating, the optimized coating, as-cast Ni-Al bronze and AISI 1020 carbon steel obtained in a medium of 3.5 wt.% NaCl aqueous solution

	Non-optimized coating	Optimized coating	As-cast Ni-Al bronze	AISI 1020 steel
Ecorr (mV)	-375	-308	-282	-613
Icorr ($\mu A.cm^{-2}$)	9.52	6.51	8.57	48.40
Rct ($\Omega.cm^2$)	2464	3707	2015	748
Rfilm ($\Omega.cm^2$)	8.25	9.58	10.37	-

Silveira et al. [87] analyzed the corrosion and cavitation resistance of FeCrMnSiNi and FeCrMnSiB coatings. Using HVOF and HVAF spraying techniques to produce coatings, the results were obtained by XRD analysis, polarization tests, and SEM. The HVAF sprayed coatings presented a lower porosity and oxide levels and higher hardness values. The HVAF process showed better cavitation and corrosion resistance, due to the lower porosity and oxide contents of the coatings. The number of oxides and pores in the coatings was crucial in their corrosive behavior by facilitating the penetration of the chloride ions through the pores, leading to a higher corrosion rate and pitting formation [87].

HVOF has been used to produce Ni alloy-based coatings. Yang et al. [88] studied Ni-Mo coatings improved by annealing treatment. A commercially available spherical Ni-Mo alloy powder was used in a commercial HVOF system. The coating was annealed in a temperature range of 400 °C to 950 °C with a heating rate of 5 °C/min for 3 h in an argon atmosphere. The coating has a dense structure without apparent pores or other defects. Post-spray annealing has a significant effect on the change in coating corrosion behavior and microstructural evolution [88]. Yang et al. [89] also compared the Ni-Mo coatings deposited by using HVOF and APS techniques. The microstructure of HVOF coating is uniform and dense, with a porosity of 0.62%, a microhardness of 474.7HV0.3, and a bonding strength of 58.8 MPa. Compared with the HVOF coating, the APS coating exhibits a lamellar structure and numerous pores/microcracks with a higher porosity of 3.28%, a lower microhardness of 300.8HV0.3, and a worse bonding strength of 40.6 MPa. The potentiodynamic polarization and EIS

results showed that the HVOF coating has better corrosion resistance in an aqueous solution of HCl than the APS coating (Table 4). The APS coating showed a higher corrosion current density, and a lower charge transfer resistance and film impedance than the HVOF coating in acidic medium. The greater number of microcracks and the greater porosity of APS coatings seem to be decisive in terms of its worse corrosion behavior in acidic medium.

Table 4 – Electrochemical parameters of HVOF and APS coatings in HCl solutions (15 wt.%)

Coating	Ecorr (mV)	Icorr ($\mu A.cm^{-2}$)	Rfilm ($\Omega.cm^2$)	Rct ($\Omega.cm^2$)
HVOF	-217.29	82.28	1591.00	90.35
APS	-219.99	119.03	90.28	10.17

Lee et al. [90] studied the tribological and corrosion behavior of HVOF sprayed Ni-based coatings with two Cr concentrations (7.15 and 16.98 wt.%) on AISI 304 steel. Static and dynamic (with friction) polarization curves were obtained in seawater. The Ni-based coating with the highest Cr content showed the highest corrosion current density in the two conditions and the highest passive current density in the static condition. The poor corrosion behavior of the Ni-based coatings with a higher Cr content is associated with the de-alloying of chromium at the grain boundaries, causing intergranular corrosion (IGC). However, the higher Cr concentration increased the pitting potential in seawater.

Mechanically alloyed Ni–10 wt.%Ti powders were deposited on a 1045 steel substrate using the high velocity oxy-fuel (HVOF) thermal spraying process [91]. The phase composition of feedstock powders was preserved during spraying, and only supersaturated Ni (Ti) solid solutions were present in the coatings. The hardness of the coatings was about 510 HV (50 g). Tafel polarisation tests performed after 1 h of immersion revealed that the corrosion behavior of HVOF Ni–Ti coatings was not affected by the substrate. However, delamination of air plasma sprayed (APS) Ni–10 wt.%Ti coatings and significant corrosion of substrate in an aqueous solution of 3.5 % NaCl were observed in similar conditions. For HVOF Ni–Ti coatings, and after 24 h of immersion, the corrosion of substrate was observed after polarization measurements in a saline solution, but no delamination of the coating occurred [91].

Hosseini et al. [92] investigated how alumina nanoparticles in the hot oxidation affected the behavior of the NiCoCrAlTaY coating. The high velocity oxygen fuel (HVOF) technique was employed to deposit coatings on a single crystal CMSX-4 Ni-based superalloy. Different amounts of α-Al_2O_3 nanoparticles (3, 6, and 9 wt.%) were added to NiCoCrAlTaY powder via a modified suspension route. With this modification, the alumina nanoparticles were adhered to the surface of the atomized metallic NiCoCrAlTaY powders with a relatively uniform distribution. The composite powder was then sprayed on the superalloy substrate by an industrial HVOF route. The cyclic hot oxidation resistance of the coatings was evaluated at 1100 °C. Results showed that the coating with 6 wt% nano-Al_2O_3 experienced significantly better oxidation performance. The presence of nano- Al_2O_3 in the coating accelerated the formation of a α-Al_2O_3 dense oxide layer and, thereby, delayed the diffusion of other elements to the surface. Adding more Al_2O_3 nanoparticles up to 9 wt.% led to an increase in porosity and surface roughness of the coating, which decreased oxidation resistance.

Rathod et al. [93] produced a CoNiCrAlY coating for protection against oxidation at elevated temperatures on the surface of the 316L by high velocity oxygen fuel (HVOF) and cold gas dynamic spray (CGDS) techniques. The phase composition, microstructure, and oxidation resistance of the coating were investigated at 900 °C in air. The CGDS coating shows a low oxide growth rate because of its low porosity, oxide content, and high hardness. CGDS coating provided excellent oxidation protective ability at 900°C in air, whereas HVOF coating showed high levels of visible defects, high oxide content, spinel type oxide, and a high oxide growth rate. An electrochemical study showed that the HVOF process provided better corrosion resistance as compared to the CGDS process.

Agglomerated and sintered WC-Co and WC-Cr_3C_2-Ni commercial powders were thermally pulverized, exploiting the HVOF technique to deposit coatings on AZ31 and AZ91 magnesium alloy substrates with a plan to use two spacing differences (320 and 400 mm) between the substrate and spraying [94]. The WC-Co coating showed the highest corrosion resistance in an aqueous solution of sodium chloride. The Az91 alloy showed a gain of almost 150 times in the Rp value without the coating; however, in comparison with the uncoated alloy, the AZ31 presented a value 17 times higher (Rp = 4.2 $k\Omega \cdot cm^2$) in the polarization resistance. The spray distance did not affect the corrosion resistance of the Mg alloy coated in saline medium. Magnesium alloys with coatings showed a gain in corrosion resistance. However, WC-Co protects the

magnesium surface from corrosion more effectively than WC-Cr_3C_2-Ni.

Kunioshi et al. [95] studied the oxidation and erosion–oxidation behavior of HVOF sprayed Ni–20Cr alloy as well as WC and Cr_3C_2 cermet coatings on a steel substrate. The erosion-oxidation tests were carried out on a rig with specimen assemblies that were rotated through a fluidized bed of erodent particles in the temperature range 500–850 °C and with erodent impact velocities of 2.5–19.5 m s^{-1}. Alumina powder (∼200 μm) was used as the erodent. The Ni–20Cr and Cr_3C_2–25 (Ni–20Cr) coatings showed a higher oxidation resistance than the WC–20Cr–7Ni coating, especially at temperatures above 800 °C. The erosion-oxidation resistance of the coatings was determined by wastage as a function of temperature. The three coatings did not show any significant change in erosion-oxidation resistance at temperatures up to 500–600 °C. At higher temperatures, wastage increased with temperature, reached a maximum at 700 °C and then decreased with further increases in temperature [95].

The coating produced by the HVOF technique presents a high influence of the characteristics of powder, where the spherical structure allows better fluidity. Besides, the low temperature and high speed do not cause significant changes in the phase and production of oxides, giving the coating a similar structure to that presented in the powder [85].

The production of coatings containing graphene, such as graphene nanoplatelets (GNP) and graphene oxide (GO), has been extensively studied due to their excellent properties, including their anticorrosion properties [96]. In view of the great potential of spray techniques to produce coatings, despite the limitation presented by the technique to the use of heat that can degrade or oxidize graphene, studies have been carried out focusing on the production of coatings made of graphene-containing composites [96].

A recent work by Forati et al. [97] studied the deposition of composite/graphene nanoplatelet (GNP) by the APS and HVOF techniques, and a major challenge found in the work was to avoid damage or oxidation of graphene at high temperatures, so the work carried out the optimization of spray conditions. A composite powder of copper and GNP particles was prepared due to graphene's inability to reach adequate speed during spraying, to the detriment of its low mass. The resulting powder has a flake-like layered structure. Spraying was carried out using different vestments for both techniques. The coating using the APS technique has a lamellar structure containing some characteristics of a flower shape. The HVOF coating showed greater homogeneity and a denser morphology. The study was able to demonstrate that by varying the spray parameters, it is possible to preserve the GNP particles by obtaining Cu-GNP composite coatings by using APS and HVOF processes. Both APS and HVOF-prepared composite coatings showed an improvement in corrosion resistance in NaCl 0.1 M [96].

Pattnayak et al. [98] developed a hard, wear-resistant ceramic-based coating containing alumina doped with 0.8% Ceria (CeO_2) and reduced graphene oxide (rGO, 0–0.2%) on 17-4 PH steel using the high-velocity oxygen fuel (HVOF) thermal spray process. The 17-4 PH steel contains chromium (15-9 -16.4 wt.%), nickel (4-4.7 wt.%, and copper (3.3-3.7 wt.%). The coating thickness varied between 318 μm and 340 μm. The lowest roughness and the highest hardness and density of coatings were found for the coating with the highest rGO content, which proved to be the most hydrophobic. Potentiodynamic polarization tests showed the lowest corrosion rate for 0.2 wt.% r-GO coating (0.00038 mm/year) which is lower than that of the 17-4 PH substrate. The best corrosion behavior of the coating with 0.2 wt.% rGO was due to its highest density and hydrophobic character. Recently, Srikanth and Bolleddu [99] observed that with an increasing percentage of rGO addition, the porosity in the WC-25wt-%Co HVOF coatings has been reduced, improving their mechanical properties.

Post-treatments were used to improve the corrosion resistance of HVOF coatings in several media. The laser surface treatment was performed on the T800 (Co-Mo-Cr-Si) and T800 based WC HVOF sprayed coatings to reduce the microstructural defects of the coatings by precise control of treatment depth with or without melting [97]. The corrosion resistance of the HVOF coatings can be improved by laser densification of the coatings by eliminating discrete splat structure and porosity. However, the improvement of resistance to microgalvanic corrosion between the WC and Co matrixes after laser treatment can be limited depending on the extent of melting of the WC within the coatings [97]. After the laser treatment, the charge transfer resistance of the T800 coatings increased in an aqueous solution of 0.5 mol/L of sulfuric acid. And the charge transfer resistance of WC-T800 coatings also increased after the laser modification up to a concentration of 21 wt.% WC due to the formation of a new phase W_2CO_4C at the WC/T800 matrix, reducing the microgalvanic activity [100].

Sealants are a post-treatment adopted to seal the porosity in thermally sprayed coatings to obtain a gain in corrosion resistance. The necessary

properties for a liquid sealant are low viscosity, high surface tension, and high wettability [101]. A problem associated with sealants is gas trapped at high pressure in the pore spaces, which can lead to a loss in the bond strength of the substrate coating. Polarization curves have been evaluated for sealed and unsealed atmospheric sprayed plasma (APS) and high-velocity oxyfuel (HVOF) WC–Co–Cr coatings in acidic and alkaline solutions [101]. Sealing was employed to reduce the corrosion current density, but the effect depended heavily on the composition of the coating phase and microstructure [101]. Our group started a project in the 90's to deposit materials from urban solid waste in steel [102]. The research started with the development of polyethylene terephthalate (PET) coatings on carbon steel. The PET powders were obtained from post-consumer carbonated beverage bottles. This was part of a project to replace the currently used lead-tin-coated steel in automobile fuel tanks. The coating technology was low-velocity flame spray (LVOF). The fuel used was propane/oxygen with a lack of oxygen of 23, 35, and 42 % relative to the stoichiometric combustion; the spray distance values tested were 14 cm, 30 cm, and 32 cm, the flame temperatures were 900 ºC, 1200 ºC and 1400 ºC [102]. The pure oxygen was added to the oxygen provided by the compressed air. The PET powder had irregular shapes and a heterogeneous size distribution, generating unmelted particles on the steel surface. As the substrate temperature increases, PET degradation and the number of bubbles increase [102].

The PET-coated samples were immersed in fuels such as gasoline, hydrated alcohol, and diesel, aiming for application as an internal coating on fuel tanks in the Brazilian automotive industry. The PET coating did not peel, and changes in color were not detected in gasoline or alcohol. However, the sample immersed in diesel oil showed a change in color due to the fuel impregnation, and the interface between the immersed and non- immersed regions was evident [102]. According to these results, PET coatings could be an alternative to the Pb-Sn coated steel used in fuel tanks.

The coatings produced by the LVOF method show good adherence to the substrate and a lower oxidation rate. Mishra et al. [103] found that a high temperature oxidation occurs in equipment ranging from gas turbines, boilers, heat treating retorts, and heat exchangers. Superalloys are used for such applications due to their excellent mechanical properties and creep resistance, but they lack resistance to oxidation. Mishra et al. [103] deposited LVOF Al_2O_3–$40TiO_2$ coatings on nickel and cobalt based super alloys. The high temperature oxidation behavior of coated and uncoated super alloys has been evaluated at 800°C for 50 cycles of one hour duration. The LVOF coating showed good adherence to the substrate, as cited. AE 435 super alloy showed the highest weight gain amongst the tested materials, whereas Al_2O_3–$40TiO_2$ coated Superco 605 super alloy showed the lowest weight gain. The better oxidation resistance of Al_2O_3–$40TiO_2$ coating might be attributed to the presence of a protective Al_2O_3 phase along with a TiO_2 phase in it.

Brar et al. [104] also sprayed Al_2O_3/13%TiO_2 as well as Al_2O_3/40%$TiO_2$by using the LVOF technique. Coatings were deposited on ASTM316 boiler steel used in power generation plants. The porosity of coatings was 2% for Al_2O_3/13 wt.% TiO_2 and was found to be 1.5% for Al_2O_3/40 wt.% TiO_2. LVOF coatings showed a lower oxidation rate.

Heat treatment is mentioned as a relevant process as a means of obtaining an increase in the mechanical and biomedical properties of thermally sprayed hydroxyapatite. Tiwari and Mishra [105] deposited hydroxyapatite onto UNS S31254 stainless steel using the low-velocity oxy-fuel (LVOF) technique. They investigated the effect of annealing heat treatments on the bacterial adhesion and bioactivity properties, corrosion performance, surface morphology, crystallinity, and mechanical properties of hydroxyapatite coatings that were subjected to annealing temperatures (400 °C, 600 °C and 800 °C) carried out for 2 hours in a muffle. At higher annealing temperatures, it was observed in the XRD that there was a development of maximum crystallinity of the coatings. However, the FESEM image of the annealed sample at 800 °C revealed some losses in the form of whisker particles in the coating. The heat-treatment did not affect the adhesion strength; on the other hand, the temperature of 600 °C influenced corrosion, with better resistance at this annealing temperature. Decreasing the concentration of the bioabsorbable tricalcium phosphate (TCP) phase after the annealing treatment led to a decrease in the bioactivity of the HAp coating. The coating with superior overall performance was annealed at 600 °C.

Wang et al. [106] produced a quasicrystalline (QC) AlCuFe coating on the AA2024 alloy using high-velocity air-fuel (HVAF) spraying. A post-treatment of annealing of the samples was performed at 400 °C for 1 h. The used annealing exerts a negligible effect on the protective properties of the HVAF coating. The coated samples showed a good adhesion strength (>12 MPa), and a corrosion current density (6.7 μA. cm^{-2}) in a 3.5% NaCl medium, lower than that of the original AA2024 alloy.

III. Future and market trends in Thermal Spraying technique

According to Allied Market Research (2021) [107], the global thermal spray coating market is expected to be around $12.7 billion with a compound annual growth rate (CAGR) of 5.9 % in the period 2020-2027. The growth of different industrial fields, including textiles, aerospace, chemical industries, and automotive, has led to an increase in the application of thermal spray techniques to produce engine components. The aerospace segment is the major contributor to the market. Due to the more aggressive service conditions in the aeronautical industry, low-pressure plasma spray (LPPS) was developed to coat the hot sections of jet engines with NiCrAlV, or Ni-Co alloys. The LPPS technique produces a low oxide content in the coatings. Jet engines are the main application of thermal spraying with hundreds of components protected and sprayed with APS or HVOF [108]

In the automotive industry, thermal spray coatings are applied to piston rings, cylinder bores, exhaust components, alternator covers, among others. The exhaust headers are metallized with aluminum by using wire-combustion process [108]. For biomedical applications, hydroxyapatite can be applied by LPPS onto the implant. Two growing areas of additive manufacturing for thermal spray are direct manufacturing of parts and tool repair. APS has been used to repair tooling such as casting molds.

Regarding the materials used, the thermal spray market covers ceramics, plastics, composites, metals, and alloys. Among these, it is expected to have the highest CAGR for metals and alloys by 2027. For the different processes of thermal spray, the flame spraying should continue from the top of the most applied and with the highest CAGR [107].

In recent decades [109], thermal barrier coatings (TBC) consisting of functionally graded material (FGM) have reduced the thermal stresses and improved the resistance of a TBC to thermal shock cracking. Several FGMs deposited by thermal spraying have been incorporated into industry. The major challenge in designing an FGM is the ability to fabricate a coating with the desired compositional variation. So far, FGM coatings have been made by using premixed powders with different ratios of the constituent phases, resulting in discrete stepwise variations. This limits production as well as design flexibility. Cost-effective technologies capable of producing continuous variations in constituent materials are required. Additionally, technologies that can create nanostructured refractory phases within the FGM can meet the requirements of future high temperature applications [106]. There are several methods for deposition of the ceramic thermal barrier coatings, including atmospheric plasma spraying (APS), solution precursor plasma spray (SPPS), electron-beam physical vapor deposition (EB-PVD), etc. For the deposition of ceramic thermal barrier coatings, the APS technique is the most used due to its high deposition rate, availability, versatility, relatively low cost, and applicability over large areas [110-115].

Efforts have been made to develop the area of thermal spraying involving universities, thermal spray equipment manufacturers, coating industries, input manufacturers in consortiums aimed at expanding and growing the technique's knowledge and applications [108].

Aiming at coatings with high resistance to corrosion in aggressive media, the lamellar morphology of thermally sprayed coatings is a great advantage as it delays the entry of aggressive agents, forcing agents to follow a more tortuous path. Other key characteristics of coatings that must be controlled to obtain efficient anti-corrosive coatings are porosity and oxide content between lamellae, for example. In this respect, the cold spray technique is advantageous, as it uses lower temperatures and presents less formation of oxides. The LVOF technique is also characterized by a lower oxidation rate. Considering that porosity is a key factor that markedly affects the corrosion resistance of the coated material, flame spray, which is the most applied technique, operates with a lower temperature and a lower spray velocity, producing coatings with a higher porosity than other methods. Also, the detonation gun spraying (DGS) method presents excellent adhesive force, low porosity, and compressive residual stresses on coating surfaces, characteristics efficient in combating the corrosion of coated materials.

References

[1] Wielage B, Hofmann U, Steinhauser S, Zimmermann G. Improving wear and corrosion resistance of thermal sprayed coatings. Surf Eng. 2013; 14:136-138. doi: 10.1179/sur.1998.14.2.136

[2] Babu PS, Madhavi Y, Krishna LR, Sivakumar G, Rao DS, Padmanmabham G. Thermal Spray Coatings for Erosion–Corrosion Resistant Applications. Trans Indian Inst Met.2020; 73:2141 - 2159. doi: 10.1007/s12666-020-02053-0.

[3] Dong H. Surface engineering of light alloys. Cambridge: Woodhead Publishing Limited; 2010.

[4] El-Eskandarany MS. Utilization of ball-milled powders for surface protective coating. Mech Alloy. 2020; 309–334. doi:10.1016/b978-0-12-818180-5.00012-1

[5] Berger LM. Hardmetals as thermal spray coatings. Powder Metall. 2007; 50 (3): 205-214. doi:10.1179/174329007X246078
[6] Mellor BG. Surface coatings for protection against wear. Cambridge: Woodhead Publishing Limited; 2006.
[7] Yin ZJ, Tao SY, Zhou XM, Ding CX. Particle in-flight behavior and its influence on the microstructure and mechanical properties of plasma-sprayed Al_2O_3coatings. J Eur Ceram Soc. 2008; 28 (6): 1143e1148.
[8] Yang G-J, Suo X-K.Micro and Nano Technologies, Advanced Nanomaterials and Coatings by Thermal Spray. New York: Elsevier; 2019.
[9] Arizmendi-Morquecho A, Castilla AC, Leyva-Porras C, Martinez JAA, Gutiérrez GV, Gutiérrez KJM, López LP. Microstructural Characterization and Wear Properties of Fe-Based Amorphous Crystalline Coating Deposited by Twin Wire Arc Spraying. Adv Mater SciEng.2014; 1: 1-14. doi:10.1155/2014/836739.
[10] Kumar R,Kumar S. Thermal spray coating: a study. Int J Eng SciRes Technol. 2018; 7: 610-617. 10.5281/zenodo.1207005
[11] Steffens HD, Babiak Z, Wewel M. Recent development in arc spraying, IEEE Trans Plasma Sci. 1990; 18 (6): 974-979.
[12] Rajasekaran B, Raman SGS, Joshi SV, Sundararajan G. Influence of detonation gun sprayed alumina coating on AA 6063 samples under cyclic loading with and without fretting. Tribol Int. 2008; 41: 315–322.
[13] Singh L, Chawla V, Grewa JS. A Review on Detonation Gun Sprayed Coatings. J Min Mater Charact Eng. 2012; 11: 243-265.
[14] Dongmo E, Wenzelburger M, Gadow R. Analysis and optimization of the HVOF process by combined experimental and numerical approaches. Surf Coat Technol. 2008; 202 (18): 4470-4478. doi:10.1016/j.surfcoat.2008.04.029.
[15] Li M, Shi D, Christofides PD. Model-based estimation and control of particle velocity and melting in HVOF thermal spray. Chem Eng Sci. 2004; 59 (22–23): 5647-5656.
[16] Verstak A, Baranovski V. Deposition of carbides byactivated combustion HVAF spraying [C]// Thermal Solution:Advances in Technology and Application. Osaka: DVS-GermanWelding Society, 2004: 551−555.
[17] Younes R, Bradai M A, Sadeddine A, Mouadji Y, Bilek A,Benabbas A. Effect of TiO2 and ZrO2 reinforcements on properties of Al2O3 coatings fabricated by thermal flame spraying. Trans Nonferrous Metals Soc China. 2016; 26(5): 1345–1352. doi:10.1016/s1003-6326(16)64237-1
[18] Chaliampalias D, Vourlias G, Pavlidou E, Skolianos S, Chrissafis K, Stergioudis G. Comparative examination of the microstructure and high temperature oxidation performance of NiCrBSi flame sprayed and pack cementation coatings,Appl Surf Sci. 2009; 255: 3605-3612. doi:10.1016/j.apsusc.2008.10.006.
[19] Li X, Zhai H, Li W, Cui S, Ning W, Qiu X. Dry sliding wear behaviors of Fe-based amorphous metallic coating synthesized by d-gun spray. JNon-Crystall Solids. 2020; 537: 120018. doi:10.1016/j.jnoncrysol.2020.120018.
[20] Karimi MR, Salimijazi HR, Golozar MA. Effects of remelting processes on porosity of NiCrBSi flame sprayed coatings. Surf Eng. 2016; 32: 238-243. doi: 10.1179/1743294415Y.0000000107
[21] Kong W, Li K, Hu J. Immersion corrosion behavior, electrochemical performance and corrosion mechanism of subsonic flame sprayed FeCoCrMoSi amorphous coating in 3.5% NaCl solution. Int J Hydrogen Energy. 2022; 47 (10): 6911-6923. doi:10.1016/j.ijhydene.2021.12.039
[22] Si C, Duan B, Zhang Q, Cai J, Wu W. Microstructure, corrosion-resistance, and wear-resistance properties of subsonic flame sprayed amorphous Fe–Mo–Cr–Co coating with extremely high amorphous rate. J Mater Res Technol. 2020; 9 (3): 3292-3303. doi:10.1016/j.jmrt.2020.01.024.
[23] Mofid MA, Nejad AM. Flame spray assisted TLP bonding of Ti alloy to Al alloy, Mater Chem Phys. 2021; 263: 124404. doi:10.1016/j.matchemphys.2021.124404.
[24] Redjdal O, Zaid B, Tabti MS, Henda K, Lacaze, PC.Characterization of thermal flame sprayed coatings prepared from FeCr mechanically milled powder. J Mater ProcessTechnol. 2013; 213: 779-790.
doi:10.1016/j.jmatprotec.2012.11.018
[25] Hidalgo VH, Varela, JB, de la Calle JM, Menéndez AC.Characterisation of nicr flame and plasma sprayed coatings for use in high temperature regions of boilers. Surf Eng 16(2): 137–142. doi:10.1179/026708400101517035
[26] BergantZ,Trdan U, Grum J. Effectof high-temperature furnace treatment on the microstructure and corrosion behavior of NiCrBSi flame-sprayed coatings. Corr Sci. 2014; 88: 372-386.
[27] Jamshidi R, Bayat O, Heidarpour A. Tribological and corrosion behavior of flame sprayed Al–10 wt% Ti3SiC2 composite coating on carbon steel. Surf Coat Technol. 2019; 358: 1-10.
[28] Torres B, Campo M, Rams J. Properties and microstructure of Al–11Si/SiCp composite coatings fabricated by thermal spray. Surf Coat Technol. 2009;203 (14): 1947-1955.

[29] Chen X, Yuan J, Huang J, Ren K, Liu Y, Lu S, Li H. Large-scale fabrication of superhydrophobic polyurethane/nano-Al2O3 coatings by suspension flame spraying for anti-corrosion applications. Appl Surf Sci. 2014; 311: 864-869.
[30] ShresthaS, Sturgeon AJ. Use of Advanced Thermal Spray Processes for Corrosion Protection in Marine Environments. Surf Eng. 2004; 20(4): 237–243. doi:10.1179/026708404225016337
[31] Mardali M, SalimiJazi HR, Karimzadeh F, Luthringer B, Blawert C, Labbaf S. Comparative study on microstructure and corrosion behavior of nanostructured hydroxyapatite coatings deposited by high velocity oxygen fuel and flame spraying on AZ61 magnesium based substrates. Appl Surf Sci. 2019; 465: 614-624.
[32] Kim M, Choi E, Lee D, Seo J, Back T-S, So J, Yun J-Y, Suh S-M. The effect of powder particle size on the corrosion behavior of atmospheric plasma spray-Y_2O_3 coating: Unraveling the corrosion mechanism by fluorine-based plasma. Appl Surf Sci. 2022; 606: 154958. doi:10.1016/j.apsusc.2022.154958.
[33] Huang B, Wang J, Tang Z, Li W, Zhu W, Gu R. Fluoride-mediated corrosion mechanism of atmospheric-plasma-sprayed yttrium–aluminium garnet ceramic coatings. J Eur Ceram Soc. 2022; 42(13): 6146-6158. doi:10.1016/j.jeurceramsoc.2022.06.01
[34] Babu A, Dzhurinskiy D, DautovS,Shornikov P. Structure and electrochemical behavior of atmospheric plasma sprayed Cr3C2-NiCr cermet composite coatings. Int J Refract Metals Hard Mater. 2023; 111: 106105. doi:10.1016/j.ijrmhm.2023.106105
[35] Meghwal A, Anupam A, Schulz C, Hall C, Murty B, Kottada R S, Vijay R, Munroe P, Berndt C C, Ang A S M. Tribological and corrosion performance of an atmospheric plasma sprayed AlCoCr0.5Ni high-entropy alloy coating. Wear. 2022; 506-507: 204443. doi:10.1016/j.wear.2022.204443
[36] Guo S, Xu D, Liang Y, Gong Y, Li Y, Yang J. Corrosion characterization of ZrO2 and TiO2 ceramic coatings via air plasma spraying on 316 stainless steel in oxygenated sub- and supercritical water. The J Supercritical Fluids. 2019; 104716. doi:10.1016/j.supflu.2019.104716
[37] Hu L, Song X, Zhao X, Guo F, Yang F,Xiao P. A robust, hydrophobic CeO2/NiCoCrAlY composite coating with excellent thermal stability and corrosion resistance prepared by air plasma spray. J Alloys Compound. 2021; 861: 158623. doi:10.1016/j.jallcom.2021.158623
[38] Wang T, Shao F, Ni J, Zhao H, Zhuang Y, Sheng J, Zhong X, Yang J, Tao S. Corrosion behavior of air plasma spraying zirconia-based thermal barrier coatings subject to Calcium–Magnesium–Aluminum-Silicate (CMAS) via burner rig test. Ceram Int. 2020; 46: 18698-18706. doi:10.1016/j.ceramint.2020.04.184
[39] ZhaoY, Ge Y, Jin X, Koch D, Vaßen R, Chen Y, Fan X. Oxidation behavior of double-ceramic-layer thermal barrier coatings deposited by atmospheric plasma spraying and suspension plasma spraying. Ceram Int. 2022; 48(16): 23938-23945. doi:10.1016/j.ceramint.2022.05.068
[40] Bakan E, Vaßen R. Oxidation kinetics of atmospheric plasma sprayed environmental barrier coatings. J EurCeram Soc. 2022; 42(12): 5122-5128. doi:10.1016/j.jeurceramsoc.2022.05.003
[41] Mao X-Y, Wang Y-X, Jiang J, Chi Y-L, Dong Y, Yang Y, He J-N. (2022) Microstructure and corrosion performance of Al0.5FeCoNiCrMn coating prepared by plasma spraying mechanically alloyed powders. Surf Eng. 2022; 38 (4): 383-392. doi:10.1080/02670844.2022.2082156
[42] Zhang Y, Gao X, Liang X, Chong K, Wu D, Zou Y. Effect of laser remelting on the microstructure and corrosion property of the arc-sprayedAlFeNbNi coatings. Surf Coat Technol. 2020; 398: 126099. doi:10.1016/j.surfcoat.2020.126099.
[43] Singh JK, Yang H-M, Lee H-S, Kumar S, Aslam F, Alyousef R, Alabduljabbar H. Morphological and corrosion studies of ammonium phosphate and caesium nitrate treated Al coating deposited by arc thermal spray process, Surf Interf. 2021; 22: 100885, ISSN 2468-0230. doi:10.1016/j.surfin.2020.100885.
[44] Haixiang C, Dejun K. Comparison on electrochemical corrosion performances of arc and laser thermal sprayed Al–Ti–Ni coatings in marine environment. MaterChem Phys. 2020; 251: 123200. doi:10.1016/j.matchemphys.2020.123200
[45] Kamal S, Jayaganthan R, Prakash S, Kumar S. Hot corrosion behavior of detonation gun sprayed Cr_3C_2–NiCr coatings on Ni and Fe-based superalloys in Na_2SO_4–60% V_2O_5 environment at 900°C. J Alloys Compound. 2008; 463, (1–2): 358-372. doi:10.1016/j.jallcom.2007.09.019.
[46] Zhai H, Yuan H, Li W, Zhang X, Li X, Cai A. Corrosion resistance mechanisms of detonation sprayed Fe-based amorphous coating on AZ31B magnesium alloy. J Non-Crystall Solids. 2022; 576: 121276. doi:10.1016/j.jnoncrysol.2021.121276.
[47] Kumar S, Handa A, Chawla V, Grover NK, Kumar R.Performance of thermal-sprayed coatings to combat hot corrosion of coal-fired boiler tube and effect of process parameters and post-coating heat treatment on coating performance: a review. Surf Eng. 2021; 37: 833-860.
[48] Talako T, Yakovleva M, Astakhov E, Letsko A. Structure and properties of detonation gun

sprayed coatings from the synthesized FeAlSi/Al_2O_3 powder. Surf Coat Technol. 2018; 353: 93-104. doi:10.1016/j.surfcoat.2018.08.063
[49] Ashokkumar M, Thirumalaikumarasamy D, Thirumal P, Barathiraja R. Influences of Mechanical, Corrosion, erosion and tribological performance of cold sprayed Coatings: A review. MaterToday*:* Proc. 2021; *46*: 7581-7587. doi:10.1016/j.matpr.2021.01.664
[50] Kumar S. Influence of processing conditions on the mechanical, tribological and fatigue performance of cold spray coating: a review. Surf Eng. 2022; 38 (4): 324-365.
doi:10.1080/02670844.2022.2073424
[51] Bai X, Tang J, Gong J, Lü X. Corrosion performance of Al–Al2O3 cold sprayed coatings on mild carbon steel pipe under thermal insulation. Chinese JChem Eng. 2017; 25 (4): 533-539. doi:10.1016/j.cjche.2016.10.004.
[52] Witharamage CS, Alrizqi MA, Chirstudasjustus J, Darwish AA, Ansell T, Nieto A, Gupta RK. Corrosion-resistant metallic coatings for aluminum alloys by cold spray.
Corr Sci. 2022; 209: 110720. doi:10.1016/j.corsci.2022.110720.
[53] Chirstudasjustus J, Felde MR, Witharamage CS, Esquivel J, Darwish AA, Winkler C, Gupta RK. Age-hardening behavior, corrosion mechanisms, and passive film of nanocrystalline Al-V alloy exhibiting supersaturated solid solution. J. Mater SciTechnol.2023; 135: 1-12.
[54] Witharamage CS, Christudasjustus J, Smith J, Gao W, Gupta RK. Corrosion behavior of an in-situ consolidated nanocrystalline Al-V alloys
npj Mater Degrad. 2022; 6: 15.
[55] Chu X, Meng F, Chi Z, Aydin H, Wei Y-K, Vo P, Sun W, Huang R, Yue S. Effects of powder characteristics and mixing powders on cold sprayability and corrosion properties of tantalum coatings. Surf Coat Technol. 2021; 426: 127763. doi:10.1016/j.surfcoat.2021.127763.
[56] Zhou S, Sun J, Bernard C, Lin H, Saito H, Miyazaki T, Ichikawa Y, Ogawa K. Interfacial oxidation and boundary amorphization deposition mechanisms of GaN powder on metallic substrate by low-pressure cold spraying. Appl Surf Sci. 2023; 614: 156221. doi:10.1016/j.apsusc.2022.156221
[57] Luo X, Wei Y, Shen J, Ma N, Li C. Breaking the trade off between corrosion resistance and fatigue lifetime of the coated Mg alloy through cold spraying submicron-grain Al alloy coatings. J Magn Alloys. 2023. doi:10.1016/j.jma.2022.12.011
[58] DaroonparvarM, Khan M F, Saadeh Y, Kay C, Kasar A, Kumar P, Esteves L, Misra M, Menezes P, Kalvala P, Bakhsheshi-Rad H,Gupta R. Modification of surface hardness, wear resistance and corrosion resistance of cold spray Al coated AZ31B Mg alloy using cold spray double layered Ta/Ti coating in 3.5 wt % NaCl solution. Corr Sci. 2020; 176: 109029. doi:10.1016/j.corsci.2020.109029
[59] Norrell T, Ferguson G, Ansell T, Saladin T, Nardi A, Nieto A. Synthesis and corrosion behavior of cold sprayed dual nanoparticle reinforced Al coatings. Surf Coat Technol. 2020; 401: 126280. doi:10.1016/j.surfcoat.2020.126280
[60] Wei Y, LuoX, Chu X, Ge Y, Huang G, Xie Y, Huang R, Li C. Ni coatings for corrosion protection of Mg alloys prepared by an in-situ micro-forging assisted cold spray: Effect of powder feedstock characteristics. Corr Sci. 2021; 184: 109397. doi:10.1016/j.corsci.2021.109397
[61] Jiang X, Overman N, Smith C, Ross K. Microstructure, hardness and cavitation erosion resistance of different cold spray coatings on stainless steel 316 for hydropower applications. Mater Today Commun. 2020; 25: 101305. doi: 10.1016/j.mtcomm.2020.101305
[62] Widener C, Hrabe R, James B, Champagne V. B1 Bomber-FEB panel repair by cold sprayCold Spray Action Teem Meet, Worcest., MA USA (2013)
[63] Champagne V, Helfritch D. Critical Assessment 11: structural repairs by cold spray.Mater Sci Technol. 2015; 31: 627-634.
doi:10.1179/1743284714Y.000000072
[64] Li W, Cao C, Wang G, Wang F, Xu Y, Yang X. 'Cold spray +' as a new hybrid additive manufacturing technology: a literature review. Sci Technol Weld Join. 2019; 24: 420-445.
doi:10.1080/13621718.2019.1603851
[65] Tang J, Saha GC, Richter P, Kondás J, Colella A, Matteazzi P. Effects of post-spray heat treatment on hardness and wear properties of Ti-WC high-pressure cold spray coatings. J Therm Spray Technol. 2018; 27: 1153-1164.
doi:10.1007/s11666-018-0762-7
[66] Yang G-J, Gao P-H, Li C-X, Li C-J. Mechanical property and wear performance dependence on processing condition for cold-sprayed WC-(nanoWC-Co). Appl Surf Sci. 2015; 332: 80-88.
doi:10.1016/j.apsusc.2015.01.138
[67] Moridi A, Hassani-Gangaraj SM, Vezzú S, Trško L, Guagliano M. Fatigue behavior of cold spray coatings: the effect of conventional and severe shot peening as pre-/post-treatment. Surf Coat Technol. 2015; 283: 247-254, doi:10.1016/j.surfcoat.2015.10.063
[68] Ghelichi R, MacDonald D, Bagherifard S, Jahed H, Guagliano M, Jodoin B. Microstructure and fatigue behavior of cold spray coated Al5052. Acta Mater.2012;60 :6555-6561. doi:10.1016/j.actamat.2012.08.020

[69] Wei Y-K, Li Y-J, Zhang Y, Luo X-T, Li C-J. Corrosion resistant nickel coating with strong adhesion on AZ31B magnesium alloy prepared by an in-situ shot-peening-assisted cold spray. Corr Sci. 2018; 138: 105-115. doi:10.1016/j.corsci.2018.04.018

[70] Al-Mangour B, Mongrain R, Irissou E, Yue S. Improving the strength and corrosion resistance of 316L stainless steel for biomedical applications using cold spray. Surf CoatTechnol. 2013; 216: 297-307. doi:10.1016/j.surfcoat.2012.11.061

[71] Bala N, Singh H, KarthikeyanJ, Prakash S. Cold spray coating process for corrosion protection: a review. Surf Eng. 2014; 30(6): 414–421. doi:10.1179/1743294413Y.0000000148

[72] Devi G N, Kumar S, Balaji T S, Mangalarapu T B, Chandrasekhar S, Gopal AV, Jyothirmayi A. Influence of inter-splat bonding state of cold sprayed IN625 and IN718 coatings on mechanical and corrosion performance. Surf Coat Technol. 2022; 445: 128731. doi:10.1016/j.surfcoat.2022.128731

[73] TripathyS, Behera A, Pati S,Roy S. Corrosion resistant nickel coating on mild steel by cold gas dynamic spraying. Mater Today: Proc. 2021; 46: 4395-4399. doi:10.1016/j.matpr.2020.09.668

[74] Wathanyu K, Tuchinda K, Daopiset S, Sirivisoot S. Corrosion resistance and biocompatibility of cold-sprayed titanium on 316L stainless steel. Surf Coat Technol. 2022; 445: 128721. doi:10.1016/j.surfcoat.2022.128721

[75] Yin S, Cizek J, Yan X, Lupoi R. Annealing strategies for enhancing mechanical properties of additively manufactured 316L stainless steel deposited by cold spray.
Surf Coat Technol.2019; 370: 353-361. doi:10.1016/j.surfcoat.2019.04.012

[76] Ralls A M, Daroonparvar M, Sikdar S, Rahman M H, Monwar M, Watson K, Kay CM, Menezes P L. Tribological and Corrosion Behavior of High Pressure Cold Sprayed Duplex 316 L Stainless Steel. Tribol Int. 2022; 169: 107471. doi:10.1016/j.triboint.2022.107471

[77] ZhuJ, Cheng X, Zhang L, Hui X, Wu Y, Zheng H, Ren Z, Zhao Y, Wang W, Zhu S, Wang X. Microstructures, wear resistance and corrosion resistance of CoCrFeNi high entropy alloys coating on AZ91 Mg alloy prepared by cold spray. J Alloys Compound. 2022; 925: 166698. doi:10.1016/j.jallcom.2022.166698

[78] YaoH, Hu X, Yi Z, Xia J, Tu X, Li S, Yu B, Zhang M, Bai X, Chen Q, Wang H. Microstructure and improved anti-corrosion properties of cold-sprayed Zn coatings fabricated by post shot-peening process. Surf Coat Technol. 2021; 422: 127557. doi:10.1016/j.surfcoat.2021.127557

[79] Wang Y, Wu M, Lu P, Zhou W, Shi X, Yang K, Miao X. Mechanical and corrosion resistance of cold sprayed zinc (CSZ) nano composite coating enhanced by SiO2-GO hybrid material. Colloids Surf A: Physicochem Eng Aspects, 2022; 632: 127824.
doi:10.1016/j.colsurfa.2021.127824

[80] WuH, Shen G, Li R, Zhang L, Jie X, Liu G. Influence of embedded reduced graphene oxide on the corrosion-wear performance of cold sprayed Zn-rGO/Al coating in NaCl solution. Surf Coat Technol. 2022; 429: 127856. doi:10.1016/j.surfcoat.2021.127856

[81] Xie C, Li H, Zhou X, Sun C. Corrosion behavior of cold sprayed pure zinc coating on magnesium. Surf Coat Technol. 2019; 374: 797-806. doi:10.1016/j.surfcoat.2019.06.068

[82] Koivuluoto H, Vuoristo P. (2014). Structure and corrosion properties of cold sprayed coatings: a review. Surf Eng. 2014; 30(6): 404–413. doi:10.1179/1743294413y.0000000201

[83] Cheng J, Wu Y, Hong S, Cheng J, Qiao L, Wang Y, Zhu S. Spray parameters optimization, microstructure and corrosion behavior of high-velocity oxygen-fuel sprayed non-equiatomicCuAlNiTiSi medium-entropy alloy coatings, Intermetall. 2022; 142: 107442. doi:10.1016/j.intermet.2021.107442.

[84] Bhushan B, Banerjee A, Patel S N, Banik D, Godbole K, Vishwanath K, Mandal S, Mondal K. Electrochemical response and passivation affinity of Fe-based amorphous HVOF coatings prepared from pig iron on mild steel. Surf CoatTechnol. 2023; 452: 129082. doi:10.1016/j.surfcoat.2022.129082

[85] Wang K, Hong S, Wei Z, Hu N, Cheng J, Wu Y. Long-term corrosion behavior of HVOF sprayed Cr3C2–NiCr coatings in sulfide-containing 3.5 wt.% NaCl solution, J Mater Res Technol. 2021; 15: 3122-3132. doi:10.1016/j.jmrt.2021.09.131.

[86] Gil L, Staia MH, Guevara R, Puchi-Cabrera ES, Lewis DB.Microstructural characterisation of NiWCrBSiC alloy coating produced by HVOF thermal spraying.Surf Eng. 2006; 22 (4): 304-313.

[87] Silveira LL, Pukasiewicz AGM, Aguiar DGM, Zara AJ, Björklund S. Study of the corrosion and cavitation resistance of HVOF and HVAF FeCrMnSiNi and FeCrMnSiBcoatings. SurfCoat Technol. 2019; 374: 910-922. doi:10.1016/j.surfcoat.2019.06.076.

[88] Yang K, Chen C, Xu G, Jiang Z, Zhang S, Liu X. HVOF sprayed Ni–Mo coatings improved by annealing treatment: microstructure characterization, corrosion resistance to HCl and corrosion mechanisms, J Mater Res Technol. 2022; 19: 1906-1921. doi:10.1016/j.jmrt.2022.05.181.

[89] Yang K, Jiang Z, Chen C, Zhang S, Liu X. Investigation on the microstructure, tribological

performance and corrosion resistance of Ni–Mo coatings deposited by HVOF and APS methods. Vacuum. 2022; 200: 111023. doi:10.1016/j.vacuum.2022.111023
[90] Lee H, Hong Y, Sheu H, Hsiao R, Li W, Lin H. Effects of Cr contents on tribological and corrosion behavior of HVOF sprayed Ni-based alloy coating. Tribol Int. 2023; 183: 108384. doi:10.1016/j.triboint.2023.108384
[91] Verdian MM. Characterisation and corrosion performance of HVOF sprayed Ni–10 wt-%Ti coatings. Surf Eng. 2014; 30(9): 670–674. doi:10.1179/1743294414Y.0000000310
[92] HosseiniY, Kermanpur A, Ashrafizadeh F, Keyvani A. Enhancing hot oxidation resistance of the HVOF-sprayed NiCoCrAlTaY coating by alumina nanoparticles via a modified suspension route. J Mater Res Technol. 2023; 22: 3387-3401. doi:10.1016/j.jmrt.2022.12.185
[93] RathodWS, Khanna AS, Karthikeyan J, Rathod RC. Oxidation and corrosion behaviour of CoNiCrAlY bond coats. Surf Eng. 2014; 30(6): 432–442. doi:10.1179/1743294414y.0000000255
[94] Jonda E, Łatka L, Godzierz M, Maciej A. Investigations of microstructure and corrosion resistance of WC-Co and WC-Cr3C2-Ni coatings deposited by HVOF on magnesium alloy substrates. Surf Coat Technol. 2023; 459: 129355. doi:10.1016/j.surfcoat.2023.129355
[95] Kunioshi CT, Correa OV, Ramanathan LV. High temperature oxidation and erosion–oxidation behaviour of HVOF sprayed Ni–20Cr, WC–20Cr–7Ni and Cr_3C_2–Ni–20Cr coatings. Surf Eng. 2006; 22(2): 121–127. doi:10.1179/174329406x98403
[96] Mulone A, Mahade S, Björklund S, Lundström D, Kjellman B, Joshi S, Klement U. Development of yttria-stabilized zirconia and graphene coatings obtained by suspension plasma spraying: Thermal stability and influence on mechanical properties. Ceram Int. 2023; 49 (6): 9000-9009. doi:10.1016/j.ceramint.2022.11.055.
[97] ForatiT, Sharifi N, Kaydanova T, Ettouil FB, Moghimian N, Pugh M, Dolatabadi A, Moreau C.Wetting and corrosion characteristics of thermally sprayed copper-graphene nanoplatelet coatings for enhanced dropwise condensation application, Carbon Trends. 2021; 3: 100018.
[98] Pattnayak A, Gupta A, Abhijith N, Kumar D, Jain J, Chaudhry V. Development of rGO doped alumina-based wear and corrosion resistant ceramic coatings on steel using HVOF thermal spray. Ceram Int. 2023. doi:10.1016/j.ceramint.2023.02.124
[99] Srikanth A, Bolleddu V. Characteristics of reduced graphene oxide (rGO) mixed HVOF-sprayed nanostructured coatings. Sur Eng. 2023; 421-432. doi:10.1080/02670844.2023.2232967
[100] Rakhes M, Koroleva E, Liu Z. Improvement of corrosion performance of HVOF MMC coatings by laser surface treatment. Surf Eng. 2011; 27(10): 729–733. doi:10.1179/1743294411Y.0000000001
[101] Lugscheider E, Jakiel P, Messerschmidt V, Beckschulte G. Subsequent sealing of thermally sprayed coatings to increase corrosion resistance. Surf Eng. 1994; 10(1): 46–51. doi:10.1179/sur.1994.10.1.46
[102] Duarte LT, Paula e Silva, EM, Branco JRT, Lins, VFC. Production and characterization of thermally sprayed polyethylene terephthalate coatings. Surf Coat Technol. 2004; 182 (2-3): 261-267.
[103] Mishra NK, Mishra SB, Kumar R. Characterisation and oxidation of LVOF sprayed Al ₂ O ₃ –40TiO ₂ coating on superalloys. Surf Eng. 2015; 31(5): 349–353. doi:10.1179/1743294414y.0000000348
[104] Brar SS, Brar GS, Chawla V. Microstructure and characterization of LVOF sprayed aluminium oxide-13% titanium dioxide and aluminium oxide-40% titanium dioxide coatings on ASTM 316 boiler steel. Mater Today: Proc. 2021; 50: 2474-2481. doi:10.1016/j.matpr.2021.10.413
[105] TiwariS, Mishra S. Post annealing effect on corrosion behavior, bacterial adhesion, and bioactivity of LVOF sprayed hydroxyapatite coating. Surf Coat Technol. 2021; 405: 126500. doi: 10.1016/j.surfcoat.2020.126500
[106] Wang C, Li Z, Lefimov MO, Mordyuk BN. Protection of AA2024 alloy against wear and corrosion by HVAF sprayed AlCuFe coating. Surf Eng. 2023. doi:10.1080/02670844.2023.2242116
[107] Allied Market Research- Thermal spray coating market (2020-2027): opportunities Analysis and Industry Forecast, 2021. Available at https://www.alliedmarketresearch.com/thermal-spray-coatings-market.
[108] Thermal Spray Technology: Accepted Practices, 2020. ASM Thermal Spray Society. https://doi.org/10.31399/asm.tb.tstap.t56040010
[109] Mohanty PS. Challenges in thermal spraying of refractory materials. Surf Eng. 2005; 21 (1): 1-4.
[110] Izadinia M, Soltani R, Sohi M H, Coyle T. Effect of using unpyrolyzed powder on mechanical properties of vertically cracked thermal barrier coatings. Surf Coat Technol. 2023; 459: 129404. doi:10.1016/j.surfcoat.2023.129404.
[111] Wang Y, Guo H B, Li Z Y, Gong S K. Segmented lanthanum cerium oxide thermal barrier coatings by atmospheric plasma spray. Surf Eng. 2009; 25 (7): 555-558.
[112] Wang Y, Li M X, Suo H L. Mechanical properties of YSZ thermal barrier coatings with

segmented structure. Surf Eng 2012; 28 (5): 329-332.
[113] Bai Y, Wang Y H, Wang Z, Fu Q Q, Han Z H. Influence of unmelted nanoparticles on properties of YSZ nano-coatings. Surf Eng 2014; 30 (8): 568-572.
[114] Lu G X, Hao L J, Cheng Z X, Ye F X. Enhancement on thermal shock resistance of TBCs with EP interlayer. Surf Eng 2014; 30 (8): 579-588.
[115] Gao M, Xu N, Zhang J, Luan S, Chang H, Hou W, Chang X. Influence of mechanical properties on thermal shock resistance of TBCs. Surf Eng 2021; 37 (5): 572-580.
[115] Keyvani A, Bahamirian M. Hot corrosion and mechanical properties of nanostructured Al_2O_3/CSZ composite TBCs. Surf Eng 2017; 33(6): 433–443. doi:10.1080/02670844.2016.1267423